

Partition and generating function zeros in adsorbing self-avoiding walks

E.J. Janse van Rensburg^{1†}

¹Department of Mathematics and Statistics, York University, Toronto, Ontario
M3J 1P3, Canada

Abstract. The Lee-Yang theory of adsorbing self-avoiding walks is presented. It is shown that Lee-Yang zeros of the generating function of this model asymptotically accumulate uniformly on a circle in the complex plane, and that Fisher zeros of the partition function distribute in the complex plane such that a positive fraction are located in annular regions centred at the origin. These results are examined in a numerical study of adsorbing self-avoiding walks in the square and cubic lattices. The numerical data are consistent with the rigorous results; for example, Lee-Yang zeros are found to accumulate on a circle in the complex plane and a positive fraction of partition function zeros appear to accumulate on a critical circle. The radial and angular distributions of partition function zeros are also examined and it is found to be consistent with the rigorous results.

AMS classification scheme numbers: 82B41, 82B23

† rensburg@yorku.ca

1. Introduction

The partition function of a lattice spin model (such as the Ising or Potts model) is a sum over all spin configurations $\{\sigma_i\}$ in a lattice Λ given by

$$Z_s(\beta, H) = \sum_{\{\sigma_i\}} e^{-\beta \mathcal{H}(\{\sigma_i\})}. \quad (1)$$

The inverse temperature is $\beta = \frac{1}{kT}$, and \mathcal{H} is the *Hamiltonian* of the model. This is a function of the *state* (configuration of lattice spins $\{\sigma_i\}$) and is given by

$$\mathcal{H}(\{\sigma_i\}) = -J \sum_{\langle i \sim j \rangle} f(\sigma_i, \sigma_j) - H \sum_i g(\sigma_i) + BC. \quad (2)$$

In this expression, $f(\sigma_i, \sigma_j)$ is a function of neighbouring spins σ_i and σ_j connected by edges $\langle i \sim j \rangle$. In the Ising model the spins take values $\sigma_i = \pm 1$ and $f(\sigma_i, \sigma_j) = \sigma_i \sigma_j$. Similarly, g is a function of the spins σ_i and in the Ising model $g(\sigma_i) = \sigma_i$. The Hamiltonian may also include terms corresponding to particular boundary conditions (denoted by BC). In Potts models, or other spin models, the functions f and g may be defined differently.

The parameter J in equation (2) is the coupling or interaction strength between adjacent spins, and the parameter H is an external (magnetic) field which couples to the spins. Typically, the partition function is expressed in terms of activities $x = e^{\beta J}$ and $y = e^{\beta H}$. If Λ is a finite lattice, then $Z_s(\beta, H)$ is a polynomial in x and y with non-negative coefficients and so it has no zeros on the positive real axes in the x -plane or in the y -plane.

The free energy of the model is given by $F_s(\beta, H) = \log Z_s(\beta, H)$. In finite lattices the singular points of $F_s(\beta, H)$ in the complex β - or H -planes are found at the zeros of $Z_s(\beta, H)$. H -plane zeros are called *Lee-Yang zeros* [33, 44] and the β - or T -plane zeros are *Fisher zeros* [13]. Lee-Yang or Fisher zeros of spin systems may have properties given by the *Lee-Yang theorem* [33, 44] which is based on the following theorem.

Theorem 1.1 (Proposition 5.1.1 in Ruelle [41]). *Let $N = \{1, 2, \dots, n\}$, $S = \{i_1, i_2, \dots, i_s\} \subseteq N$ and $S' = N \setminus S$. Let $t^S = \prod_{j=1}^s t_{i_j}$ where $t_k \in \mathbb{C}$. Suppose that $\{A_{ij}\}_{i \neq j}$ is a family of real numbers such that $|A_{ij}| \leq 1$ for $i, j \in N$.*

Define the polynomial

$$P_n(t_1, t_2, \dots, t_n) = \sum_{S \subseteq N} t^S \left(\prod_{i \in S} \prod_{j \in S'} A_{ij} \right).$$

Then, if $P_n(t_1, t_2, \dots, t_n) = 0$ and $|t_j| \geq 1$ for $1 \leq j \leq n-1$, it follows that $|t_n| \leq 1$. \square

A corollary of this theorem is the Lee-Yang theorem [33], namely

Theorem 1.2 (The Lee-Yang theorem – Theorem 5.1.2 in Ruelle [41]). *Let $N = \{1, 2, \dots, n\}$, $S = \{i_1, i_2, \dots, i_s\} \subseteq N$ (so that $s = |S|$) and $S' = N \setminus S$. Suppose that $\{A_{ij}\}_{i \neq j}$ is a family of real numbers such that $|A_{ij}| \leq 1$ for $i, j \in N$.*

Define the polynomial

$$P_n(t) = \sum_{S \subseteq N} t^S \left(\prod_{i \in S} \prod_{j \in S'} A_{ij} \right).$$

Then the zeros of $P_n(t)$ all lie on the unit circle $|t| = 1$ in the t -plane. \square

For example, if $A_{ij} = \alpha$ for all i, j in theorem (1.2), $\alpha \in \mathbb{R}$ and $|\alpha| \leq 1$, then the zeros of the polynomial

$$P(t) = \sum_{S \in \mathcal{N}} \alpha^{s(n-s)} t^s = \sum_{s=0}^n \binom{n}{s} \alpha^{s(n-s)} t^s.$$

all lie on the unit circle $|t| = 1$ in the t -plane.

According to the Lee-Yang theorem, the zeros of the partition function of a wide class of lattice spin and related models (including the lattice gas and the Ising model) lie on the unit circle in the complex $y = e^{\beta H}$ plane. In the thermodynamic limit the Lee-Yang zeros accumulate on the unit circle, with a density profile which determines the critical behaviour in the model. The Lee-Yang zeros approach the positive real axis in the y -plane, creating an *edge singularity* at the critical value of the magnetic field H . This edge singularity is now known to be associated with a ϕ^3 scalar field theory [15], and has been studied in the context of a wide variety of lattice models, including the n -vector model [31], the q -state Potts model [28, 30], and also for a two dimensional ϕ^3 theory [7].

In contrast to Lee-Yang zeros, the zeros in the complex temperature plane may not be distributed on the unit circle (in the complex $x = e^{\beta J}$ plane). More generally, they are distributed in ways which depend on the model, and are useful in understanding phase transitions [14]. In the Ising model with special boundary conditions these zeros accumulate on two circles in the complex x -plane [4, 14]. These circles correspond to the ferromagnetic and anti-ferromagnetic phases. This pattern is not seen in the q -state Potts model when $q > 2$ [29, 30].

The partition function zeros of models of lattice clusters have received far less attention in the literature. Some results which are related to the Lee-Yang singularities in spin systems are known. For example, the Lee-Yang edge singularity of the Ising model in an imaginary magnetic field in d dimensions was shown to be related to critical behaviour in a model of lattice trees in $d+2$ dimensions (see reference [38]), giving exact values for the lattice tree entropic exponent in two and in three dimensions. Partition function zeros of collapsing self-avoiding walks were studied in references [32, 40], and considered for adsorbing walks in reference [35, 42, 43].

In this paper the properties of Lee-Yang and Fisher zeros in a model of adsorbing self-avoiding walks are considered. Firstly, theorems about the distribution of polynomial zeros can be used to prove results on the distribution of generating and partition function zeros. These theorems include classical theorems by Erdős and Turán [12], and also newer results in references [20] and [11]. Secondly, by using the GAS algorithm [24, 26] to estimate microcanonical data on adsorbing walks, a numerical approach to study the distribution of Lee-Yang zeros is presented.

The paper is organised as follows.

In section 2 a short review of models of adsorbing walks is given. In particular, the partition function, generating function and free energy is defined, and partial sums of the generating function is introduced.

In sections 2.2 and 2.4 the properties of zeros of partial sums of the generating function are presented, while partition function zeros (Fisher zeros) are examined in section 2.3.

In general the partition function of interacting models of connected clusters (walks, polygons or animals) in a lattice is of the form

$$Z_n(a) = \sum_{m \geq 0} q_n(m) a^m \quad (3)$$

where $q_n(m)$ is the number of clusters of size n and energy m . The zeros $\{a_k\}$ of $Z_n(a)$ are *Fisher zeros* (or partition function zeros). While the results in section 2.3 are directly applicable to the model of adsorbing walks in this paper, it is also the case that similar approaches can be used in other models.

The partition function $Z_n(a)$ is a polynomial in a , and so it factors such that the (extensive) free energy of the model is given by

$$f_n(a) = \log Z_n(a) = \log C + \sum_{k \geq 0} \log(a - a_k) \quad (4)$$

where $\log C$ is an analytic (background) contribution to $f_n(a)$. At each zero a_k there is a branch point in $f_n(a)$ in the complex a -plane, and, by taking the thermodynamic limit $n \rightarrow \infty$, these singular points distribute in the a -plane and create edge-singularities on the positive real a -axis. These edge-singularities correspond to phase transitions in the model [33, 41, 44]. It is shown in this paper that, for adsorbing walks, a positive fraction of partition function zeros accumulate in an annulus with centre at the origin (see theorem 2.8), and that the angular distribution of the zeros is bounded (see theorem 2.11) in the thermodynamic limit.

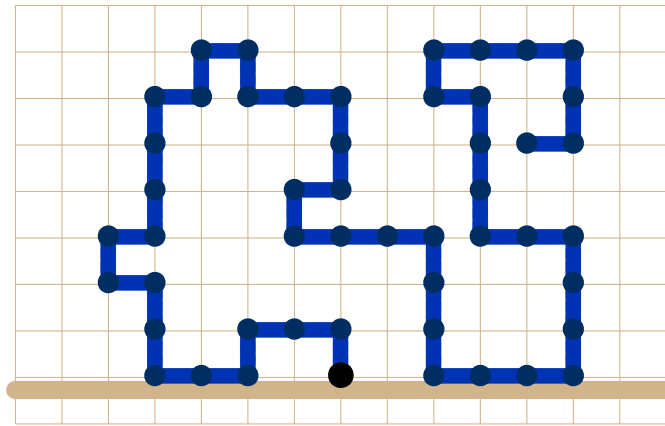
Related to the above are zeros of the generating function

$$G(a, t) = \sum_{n \geq 0} Z_n(a) t^n. \quad (5)$$

These are studied in sections 2.2 and 2.4 by considering partial sums of the generating function, and examining the properties of t -plane zeros (these are *Lee-Yang zeros*) or the properties of a -plane zeros (these are *Yang-Lee zeros*). Lee-Yang zeros are shown to accumulate on a circle in the t -plane for models of adsorbing walks (see theorems 2.2 and 2.4), while Yang-Lee zeros in the a -plane are found to have properties similar to the partition function zeros examined in section 2.3.

The numerical determination of the location of partition function zeros are examined in section 3 and the properties of the square and cubic lattice adsorbing walk partition function and generating function zeros are considered numerically in sections 4 and 5, respectively. The Lee-Yang zeros are found to distribute evenly on a circle in the t -plane (approaching a uniform distribution with increasing length of the walks), while partition function zeros are more widely distributed. It appears that a fraction of partition function zeros accumulate on a circle of critical radius in the a -plane. Similar results are found for Yang-Lee zeros in the a -plane. In addition, the trajectories of the leading partition function zeros were estimated, as well as the radial and angular distribution of partition function and Yang-Lee zeros.

Some final comments are made in the conclusions in section 6.



2. Lee-Yang and Fisher zeros in adsorbing self-avoiding walks

Let \mathbb{L}^d be the d -dimensional hypercubic lattice, and define the half-lattice $\mathbb{L}_+^d = \{\langle \vec{u} \sim \vec{v} \rangle \in \mathbb{L}^d \mid u_d \geq 0 \text{ and } v_d \geq 0\}$ where $\langle \vec{u} \sim \vec{v} \rangle$ is a lattice edge between adjacent vertices \vec{u} and \vec{v} , and u_d is the d -th component of \vec{u} . The boundary of \mathbb{L}_+^d is denoted by $\partial\mathbb{L}_+^d$ and it is a $(d-1)$ -dimensional hypercubic lattice containing the origin $\vec{0}$.

The total number of positive walks from the origin in \mathbb{L}_+^d is $c_n^+ = \sum_v c_n^+(v)$. The expected asymptotic behaviour of c_n^+ is given by

$$c_n^+ \simeq B n^{\gamma_1-1} \mu_d^n \quad (6)$$

The partition function of a model of adsorbing self-avoiding walks is given by

$$A_n^+(a) = \sum_{\nu=0}^n c_n^+(\nu) a^\nu \quad (7)$$

The thermodynamic limit of this model is given by the limit

$$\mathcal{A}^+(a) = \lim_{n \rightarrow \infty} \frac{1}{n} F_n(a) = \lim_{n \rightarrow \infty} \frac{1}{n} \log A_n^+(a). \quad (8)$$

This was shown in reference [18], and see section 9.1 in reference [23] for more results on this model. $\mathcal{A}^+(a)$ is a convex function of $\log a$. Of particular interest in this model is the existence of a critical value a_c^+ of the activity a where the walk adsorbs onto $\partial\mathbb{L}_+^d$. It is known that $\mathcal{A}^+(a)$ is not analytic at a_c^+ , that $a_c^+ < \frac{\mu_d}{\mu_{d-1}}$ (see, for example, corollary 9.3 in reference [23]) and that $a_c^+ > 1$ (see theorem 9.10 in reference [23], or reference [21] for adsorbing lattice polygons). In \mathbb{L}_+^2 series enumeration gives $a_c^+ = 1.77564 \dots$ [2] and Monte Carlo simulations in \mathbb{L}_+^3 give $a_c^+ = 1.306(7)$ [24].

It is known that [18]

$$\mathcal{A}^+(a) \begin{cases} = \log \mu_d, & \text{if } a \leq a_c^+; \\ > \log \mu_d, & \text{if } a > a_c^+. \end{cases} \quad (9)$$

The *energy* (or density of visits) $\mathcal{V}(a) = \lim_{n \rightarrow \infty} \frac{1}{n} \langle v_n \rangle$ (where $\langle v_n \rangle$ is the expected number of visits for walks of length n) is the order parameter of the model. By convexity it follows that $\mathcal{V}(a) = a \frac{d}{da} \mathcal{A}^+(a) = 0$ if $0 < a < a_c^+$ (this is the *desorbed phase*), and $\mathcal{V}(a) = a \frac{d}{da} \mathcal{A}^+(a) > 0$ if $a > a_c^+$ (whenever $\mathcal{A}^+(a)$ is differentiable – this is the *adsorbed phase*). Notice that $\mathcal{A}^+(a)$ is differentiable for almost all $a > 0$.

In the desorbed phase the walk tends to make few visits in the adsorbing plane $\partial\mathbb{L}_+^d$ (on average, $o(n)$ for walks of length n). That is, in the desorbed phase the walk tends to drift away from $\partial\mathbb{L}_+^d$ and explores the bulk of the lattice \mathbb{L}_+^d . In the adsorbed phase $\mathcal{V}(a) > 0$, and the walk returns to $\partial\mathbb{L}_+^d$ with positive frequency. These two phases are separated by the adsorption critical point a_c^+ .

The asymptotic behaviour of $A_n^+(a)$ are given by expressions similar to equation (6). In particular, it is expected that

$$A_n^+(a) \sim \begin{cases} B_- n^{\gamma_1-1} \mu_d^n, & \text{desorbed phase } (a < a_c^+); \\ B_0 n^{\gamma_s-1} \mu_d^n, & \text{critical point } (a = a_c^+); \\ B_+ n^{\gamma^{(d-1)}-1} e^{n\mathcal{A}^+(a)}, & \text{adsorbed phase } (a > a_c^+). \end{cases} \quad (10)$$

The exponent γ_s is a *surface exponent* and has exact value $\gamma_s = \frac{93}{64}$ in two dimensions [5]. In three dimensions, it was estimated that $\gamma_s = 1.304(16)$ [34, 37]. In the adsorbed phase the exponent $\gamma^{(d-1)}$ is the entropic of exponent of self-avoiding walks in one dimension lower.

The scaling of $\mathcal{A}^+(a)$ is controlled by the crossover exponent ϕ which has exact value $\frac{1}{2}$ in two dimensions [1, 5], and mean field value $\frac{1}{2}$ [5]. It is thought to have value $\frac{1}{2}$ in all dimensions $d \geq 2$ and in $d = 3$ was estimated to be $\phi = 0.505(6)$ [24]. Since there is a bulk entropy contribution of $\log \mu_d$ in \mathbb{L}_+^d , the free energy scales as

$$\mathcal{A}^+(a) \sim \log \mu_d + \frac{1}{n} f_a(n^\phi (a - a_c^+)), \quad (11)$$

where f_a is a scaling function such that $f_a(x) = 0$ if $a < a_c^+$.

The *grand partition* or *generating function* of adsorbing walks is defined by

$$G(a, t) = \sum_{n=0}^{\infty} A_n^+(a) t^n = \sum_{n=0}^{\infty} \sum_{v=0}^n c_n(v) a^v t^n. \quad (12)$$

The circle of convergence of $G(a, t)$, in the t -plane, is evidently given by $|t| = e^{-\mathcal{A}^+(a)}$, since by the root test, $G(a, t)$ is convergent if

$$|t| < t_c = \lim_{n \rightarrow \infty} |A_n^+(a)|^{-1/n}. \quad (13)$$

There is a singular point in $G(a, t)$ on the positive real axis at t_c , and, if $a > 0$, then $t_c = e^{-A^+(a)}$ by equation (8). In the desorbed phase $a \in [0, a_c^+)$ and $t_c = \mu_d^{-1}$, by equation (9).

The partial sums of the generating function is defined by

$$G_N(a, t) = \sum_{n=0}^N A_n^+(a) t^n = \sum_{n=0}^N \sum_{v=0}^n c_n(v) a^v t^n \quad (14)$$

so that $G_N \rightarrow G$ as $N \rightarrow \infty$ and $|t| < t_c$. For fixed N and a , $G_N(a, t)$ is a polynomial with non-negative coefficients, and is non-decreasing along the positive real axis. The grand potential of walks of length at most N is $\log G_N(a, t)$. This is singular at the zeros of $G_N(a, t)$. Recovering $\log G(a, t)$ by taking $N \rightarrow \infty$ shows that a singular point develops on the real axis at t_c . This is an *edge-singularity*, which is the result of t -plane singular points in $G_N(a, t)$ converging to the real axis at t_c as $N \rightarrow \infty$.

2.2. Lee-Yang zeros

Theorem 1.2 is very useful in analysing lattice spin systems, such as the lattice gas [41]. However, it seems more difficult to apply this result to a model of adsorbing self-avoiding walks. Instead, one could use the theorem by Hughes and Nikechbali [20], which will be stated below.

Let $P(t)$ be a polynomial with zeros $\langle t_1, t_2, \dots, t_N \rangle$. Follow reference [20] and proceed by defining two functions ν_N and α_N to measure the distribution of zeros:

$$\begin{aligned} \nu_N(\rho) &= \#\{t_k \mid (1-\rho) \leq |t_k| \leq \frac{1}{1-\rho}\}; \\ \alpha_N(\theta, \phi) &= \#\{t_k \mid \theta < \text{Arg } t_k \leq \phi\}. \end{aligned} \quad (15)$$

Here $\text{Arg } t_k$ is the principal argument of t_k in the t -plane. Then $\nu_N(\rho)$ is the number of zeros in a thin annulus about the unit circle (and of width $2\rho + O(\rho^2)$). If the zeros cluster about the unit circle, then $\nu_N(\rho) \simeq N$ as $N \rightarrow \infty$, for small ρ . If $\lim_{N \rightarrow \infty} \frac{1}{N} \nu_N(\rho) = 1$ for any $\rho \in (0, 1)$, then almost all the zeros accumulate on the unit circle in the t -plane as $N \rightarrow \infty$.

The function $\alpha_N(\theta, \phi)$ is a measure of the angular distribution of zeros. If the distribution is uniform in the limit that $N \rightarrow \infty$, then $\lim_{N \rightarrow \infty} \frac{1}{N} \alpha_N(\theta, \phi) = \frac{1}{2\pi} (\phi - \theta)$ for $-\pi \leq \theta < \phi \leq \pi$.

Theorem 2.1 (Hughes and Nikechbali; see theorem 3 in [20]). *Let $\langle a_k \rangle$ be a sequence of complex numbers such that $a_0 a_N \neq 0$. Let $P(t) = \sum_{n=0}^N a_n t^n$. Define*

$$L_N = \log \sum_{n=0}^N |a_n| - \frac{1}{2} \log |a_0| - \frac{1}{2} \log |a_N|.$$

Then, for $0 < \rho < 1$,

$$1 - \frac{1}{N} \nu_N(\rho) \leq \frac{2}{N\rho} L_N.$$

In, particular, if $L_N = o(N)$, then $\lim_{N \rightarrow \infty} \frac{1}{N} \nu_N(\rho) = 1$ for any $\rho \in (0, 1)$. □

Theorem 2.1 may be applied to the model of adsorbing walks. Assume that the asymptotic behaviour of $A_n^+(a)$ is as given in equation (10). Define

$$\lambda_a = \begin{cases} \mu_d, & \text{if } a \leq a_c^+; \\ e^{A^+(a)}, & \text{if } a > a_c^+. \end{cases} \quad (16)$$

By equation (8),

$$\lim_{n \rightarrow \infty} \left[\frac{A_n^+(a)}{\lambda_a^n} \right]^{1/n} = 1, \quad \text{and } A_n^+(a) = \lambda_a^{n+o(n)}. \quad (17)$$

Replace t by $\lambda_a^{-1}t$ in equation (14) to define the partial sum

$$g_N(a, t) = \sum_{n=0}^N \left(\frac{A_n^+(a)}{\lambda_a^n} \right) t^n. \quad (18)$$

Taking $N \rightarrow \infty$ gives a generating function with circle of convergence $|t| = 1$ for any finite $a > 0$.

Put $a_n = \frac{A_n^+(a)}{\lambda_a^n}$ in theorem 2.1. Then the function L_N becomes

$$L_N = \log \sum_{n=0}^N \left| \frac{A_n^+(a)}{\lambda_a^n} \right| - \frac{1}{2} \log 1 - \frac{1}{2} \log \left| \frac{A_N^+(a)}{\lambda_a^N} \right|.$$

Since $A_n^+(a) = \lambda_a^{n+o(n)}$, this becomes

$$L_N \leq \log((N+1) \lambda_a^{m_N}) + \frac{1}{2} \log \lambda_a^{o(N)}$$

where m_N is that value of $o(n)$ which maximizes $\left| \frac{A_n^+(a)}{\lambda_a^n} \right| = \left| \lambda_a^{o(n)} \right|$ (and so $m_N = o(N)$). Divide by N and take $N \rightarrow \infty$ to see that

$$\lim_{N \rightarrow \infty} \frac{1}{N} L_N = 0 \quad (19)$$

and so $L_N = o(N)$. It follows by theorem 2.1 that $\lim_{N \rightarrow \infty} \frac{1}{N} \nu_N(\rho) = 1$ for any $\rho \in (0, 1)$, and so the t -plane zeros of the partial generating function $g_N(a, t)$ cluster on the unit circle as $N \rightarrow \infty$. The result is the following corollary of theorem 2.1:

Theorem 2.2. *The zeros of $g_N(a, t)$ converge on the unit circle $|t| = 1$ in the t -plane as $N \rightarrow \infty$ in the sense that, for any $\rho \in (0, 1)$ and $\epsilon > 0$, there is an N_0 such that for all $N \geq N_0$, $|1 - \frac{1}{N} \nu_N(\rho)| < \epsilon$.* \square

This implies that the zeros of $G_N(a, t)$ accumulate on the circle $|t| = \lambda_a^{-1}$ as $N \rightarrow \infty$. Hence, if

$$\psi_N(\rho) = \#\{t_k | (1-\rho)\lambda_a^{-1} \leq |t_k| \leq \frac{1}{1-\rho}\lambda_a^{-1}\}, \quad (20)$$

then a corollary of theorem 2.2 is

Corollary 2.2.1. *The zeros of $G_N(a, t)$ converge on the circle $|t| = \lambda_a^{-1}$ in the t -plane as $N \rightarrow \infty$ in the sense that, for any $\rho \in (0, 1)$ and $\epsilon > 0$, there is an N_0 such that for all $N \geq N_0$, $|1 - \frac{1}{N} \psi_N(\rho)| < \epsilon$.* \square

That is, $\lim_{N \rightarrow \infty} \frac{1}{N} \psi_N(\rho) = 1$ for any $\rho \in (0, 1)$.

The angular distribution of zeros can be considered using a theorem of Erdős and Turán which is similar to theorem 2.1 above.

Theorem 2.3 (Erdős and Turán [12]). Suppose $\langle a_n \rangle$ is a sequence in \mathbb{C} and suppose that $a_0 a_N \neq 0$. Define $P(t) = \sum_{n=0}^N a_n t^n$. Define

$$L_N = \log \sum_{n=0}^N |a_n| - \frac{1}{2} \log |a_0| - \frac{1}{2} \log |a_N|.$$

Then

$$\left| \frac{1}{N} \alpha_N(\theta, \phi) - \frac{1}{2\pi} (\phi - \theta) \right|^2 \leq \frac{C}{N} L_N,$$

for some constant C . □

A corollary of the Erdős and Turán theorem for adsorbing walks is a consequence of equation (19). Since $\frac{1}{N} L_N \rightarrow 0$ as $N \rightarrow \infty$, the result is that $\frac{1}{N} \alpha_N(\theta, \phi) \rightarrow \frac{1}{2\pi} (\phi - \theta)$. That is, the principal arguments of t -plane zeros are asymptotically uniformly distributed over angles about the origin.

Theorem 2.4. The arguments of the zeros of $G_N(a, t)$ approach a uniform distribution over angles about the origin in the sense that, for any $-\pi \leq \theta < \phi \leq \pi$ and $\epsilon > 0$, there is an N_1 such that for all $N \geq N_1$, $|\frac{1}{N} \alpha_N(\theta, \phi) - \frac{1}{2\pi} (\phi - \theta)|^2 \leq \epsilon$. □

Thus, by theorems 2.2 and 2.4 the t -plane zeros of the partial generating function $G_N(a, t)$ are uniformly distributed on the circle of radius λ_a^{-1} in the limit as $N \rightarrow \infty$. In the thermodynamic limit this circle is a natural boundary of $G(a, t)$ in the t -plane, and the point λ_a^{-1} on the positive real axis is an edge singularity.

2.3. Fisher zeros

Let $\langle a_j \rangle$ be the set of zeros of $A_n^+(a)$ in the complex a -plane. Since $A_n^+(a)$ is a polynomial of degree n in a , there are n such zeros, counted with multiplicity. The *leading zero* will always be denoted by a_1 , and it is defined as that zero with smallest positive principal argument.

By the fundamental theorem of algebra $A_n^+(a)$ factors into a product over linear factors of the form

$$A_n^+(a) = C \prod_{j=1}^n (a - a_j). \quad (21)$$

The coefficients in (the polynomial) $A_n^+(a)$ are all positive integers, so the zeros a_j are all in pairs of complex conjugates or are real, and, since $A_n^+(a)$ is a polynomial with non-negative coefficients, none of the a_j are located on the positive real axis in the complex a -plane.

The coefficient of a^n is equal to $c_n^+(n) = c_n^{(d-1)}$ (the number of walks from the origin in $\partial \mathbb{L}_+^d \equiv \mathbb{L}^{(d-1)}$, and this fixes the constant $C = c_n^{(d-1)}$. The (finite size extensive) free energy $F_n(a)$ is given by

$$F_n(a) = \log A_n^+(a) = \log c_n^{(d-1)} + \sum_{j=1}^n \log(a - a_j). \quad (22)$$

$F_n(a)$ is a non-analytic function of a but is analytic on points along the positive real axis. Dividing by n and taking $n \rightarrow \infty$ shows that the limiting free energy is given by

$$\mathcal{F}(a) = \lim_{n \rightarrow \infty} \frac{1}{n} F_n(a) = \log \mu_{d-1} + \varrho(a), \quad (23)$$

where the limit

$$\varrho(a) = \lim_{n \rightarrow \infty} \frac{1}{n} \sum_{j=1}^n \log(a - a_j) \quad (24)$$

exists and is the limiting average of $\log(a - a_j)$ taken over the zeros of $A_n^+(a)$. This limit exists for $a > 0$ since $\mathcal{F}(a)$ is known to exist in this model [18]. Since $\varrho(a)$ is analytic on a line segment in the complex a -plane, its analytic continuation into the complex a -plane is unique up to natural boundaries, by the coincidence principle.

2.3.1. The distribution of Fisher zeros: Define the plane measure of a complex set $E \subseteq \mathbb{C}$ by noting that $\mathbb{C} \simeq \mathbb{R}^2$ and by considering E to be a subset of \mathbb{R}^2 by inclusion. This endows \mathbb{C} with (real valued) plane measure α and a σ -algebra of α -measure sets.

The distribution of Fisher zeros in the a -plane will be analysed by constructing a probability measure on \mathbb{C} which is absolutely continuous with respect to plane measure α .

Suppose that $\langle h_n(a) \rangle$ is a family of (non-negative, real-valued and normalised) distribution functions on the complex a -plane with respect to plane measure α , and with the property that

$$\lim_{n \rightarrow \infty} h_n(a) = 0, \quad \text{if } |a| > 0. \quad (25)$$

Then a distribution function on the j -th zero a_j of $A_n^+(a)$ is given by $h_{j,n}(a) = h_n(a - a_j)$.

A distribution function $H_n(a)$ on the set of zeros $\{a_j\}$ may be defined by

$$H_n(a) = \frac{1}{n} \sum_{j=1}^n h_{j,n}(a). \quad (26)$$

$H_n(a)$ may be used to define a set function λ_n on plane measurable sets E in \mathbb{C} :

$$\lambda_n E = \int_E H_n(a) d\alpha(a) = \frac{1}{n} \int_E \sum_{j=1}^n h_{j,n}(a) d\alpha(a). \quad (27)$$

Notice that $\lambda_n E = 0$ if $\alpha E = 0$, that $\lambda_n E \leq \lambda_n F$ if $E \subseteq F$ and $\lambda_n E \cup F = \lambda_n E + \lambda_n F$ if $E \cap F = \emptyset$. This shows that λ_n is a complete measure on α -measure sets in \mathbb{C} . Since $\lambda_n \mathbb{C} = 1$, it is also a probability measure on α -measure sets in \mathbb{C} and it is absolutely continuous with respect to plane measure α .

There is a great deal of freedom in constructing the measure λ_n . In this paper two examples of the measure λ_n are considered:

- Define the family of functions

$$f_n(a) = \begin{cases} \frac{\tau_n}{\pi}, & \text{if } |a| \leq \frac{1}{\sqrt{\tau_n}}; \\ 0, & \text{otherwise,} \end{cases} \quad (28)$$

where $\tau_n > 0$ is a non-decreasing function such that $\tau_n \rightarrow \infty$ as $n \rightarrow \infty$. Then $f_n(a) \rightarrow 0$ if $|a| > 0$ and $n \rightarrow \infty$. Put $f_{j,n}(a) = f_n(a - a_j)$ and define the measure μ_n by

$$\mu_n E = \frac{1}{n} \int_E \sum_{j=1}^n f_{j,n}(a) d\alpha(a) \quad (29)$$

on the σ -algebra of α -measurable sets E .

- Similarly, define the family of Gaussians on \mathbb{C} by

$$g_n(a) = \tau_n e^{-\pi \tau_n |a|^2}, \quad (30)$$

where $\tau_n > 0$ is a non-decreasing function such that $\tau_n \rightarrow \infty$ as $n \rightarrow \infty$. Notice that $g_n(a) \rightarrow 0$ if $|a| > 0$ and $n \rightarrow \infty$. Define $g_{j,n}(a) = g_n(a - a_j)$ and define the measure ν_n by

$$\nu_n E = \frac{1}{n} \int_E \sum_{j=1}^n g_{j,n}(a) d\alpha(a) \quad (31)$$

on the σ -algebra of α -measurable sets E .

Then both $\mu_n \ll \alpha$ and $\nu_n \ll \alpha$ and one may choose $\lambda_n = \mu_n$, or $\lambda_n = \nu_n$ in what follows.

Existence of the limit

$$\lambda E = \lim_{n \rightarrow \infty} \lambda_n E \quad (32)$$

for arbitrary α -measure sets E is dependent on the model and the choice of λ_n , and may be difficult to prove. We assume that λ is defined in this way, and that this limit exists, and will have this as a condition in the theorems below.

If λ exists, then it is monotone. This follows because, if $E \subseteq F$, then $\lambda_n E \leq \lambda_n F$ for all values n . This shows that $\lambda E \leq \lambda F$ if $E \subseteq F$. In addition, if $E \cap F = \emptyset$, then $\lambda_n E \cup F = \lambda_n E + \lambda_n F$ for all values of n , and so it follows that $\lambda E \cup F = \lambda E + \lambda F$. Thus, λ is additive over the unions of disjoint sets. In addition, $\lambda \emptyset = 0$ and $\lambda \mathbb{C} = 1$. Hence, λ is a complete probability measure on \mathbb{C} (on the σ -algebra of α -measure sets).

Lemma 2.5. *If the limit $\lambda E = \lim_{n \rightarrow \infty} \lambda_n E$ exists for all α -measure sets E , then the set function λ is a complete probability measure on the σ -algebra of α -measure sets in \mathbb{C} .* \square

Since λ_n is absolutely continuous with respect to plane measure α on \mathbb{C} , it follows (by the Radon-Nikodym theorem) that there exist non-negative distribution functions p and p_n , unique up to zero α -measure sets, such that for any α -measure set E in \mathbb{C} ,

$$\lambda E = \int_E p d\alpha, \quad \text{and} \quad \lambda_n E = \int_E p_n d\alpha. \quad (33)$$

It is next shown that $p_n \rightarrow p$ in measure. Define set functions β_n on α -measure sets E by

$$\beta_n E = (\lambda_n - \lambda) E = \int_E (p_n - p) d\alpha. \quad (34)$$

The β_n are signed measures on \mathbb{C} . Assuming that λ is defined by equation (32) it follows that

$$\lim_{n \rightarrow \infty} \beta_n E = \lim_{n \rightarrow \infty} (\lambda_n - \lambda) E = 0 \quad (35)$$

for any α -measure set E .

The Hahn decomposition of $\mathbb{C} \simeq \mathbb{R}^2$ by the measure β_n decomposes \mathbb{C} in a positive set $F_+^{(n)}$ and a negative set $F_-^{(n)}$. Define the mutually singular (positive) measures β_n^+ and β_n^- on the Hahn decomposition of \mathbb{C} :

$$\beta_n^+ E = \beta_n(E \cap F_+^{(n)}), \quad \text{and} \quad \beta_n^- E = -\beta_n(E \cap F_-^{(n)}). \quad (36)$$

Then it follows that $\beta_n = \beta_n^+ - \beta_n^-$ is a Jordan decomposition of the signed measure β_n . Since $\lim_{n \rightarrow \infty} \beta_n E = 0$ for any α -measure set E , it follows that $\lim_{n \rightarrow \infty} \beta_n^+ E = 0$ and $\lim_{n \rightarrow \infty} \beta_n^- E = 0$ for any α -measure set E .

The total variation of the signed measure β_n is given by

$$|\beta_n| = \beta_n^+ + \beta_n^- \quad (37)$$

and it is a measure on the σ -algebra of α -measure sets in \mathbb{C} . It follows that $\lim_{n \rightarrow \infty} |\beta_n| E = 0$ for any α -measure set E . Notice that

$$\begin{aligned} |\beta_n| E &= \beta_n(E \cap F_+^{(n)}) - \beta_n(E \cap F_-^{(n)}) \\ &= \int_{E \cap F_+^{(n)}} (p_n - p) d\alpha + \int_{E \cap F_-^{(n)}} (p - p_n) d\alpha \\ &= \int_E |p_n - p| d\alpha. \end{aligned} \quad (38)$$

Since $\lim_{n \rightarrow \infty} |\beta_n| E = 0$ for every α -measure set E in \mathbb{C} , it follows that

$$\lim_{n \rightarrow \infty} \int_E |p_n - p| d\alpha = 0. \quad (39)$$

Choosing $E = \mathbb{C}$ shows that $\|p_n - p\|_1 \rightarrow 0$ in the normed space $L^1(\alpha)$. That is, if the distribution functions p_n and p exist, then p_n converges to p in the $L^1(\alpha)$ norm. This gives the lemma:

Lemma 2.6. *Suppose that the limit $\lambda E = \lim_{n \rightarrow \infty} \lambda_n E$ exists. Then there exists distribution functions p and p_n such that*

$$\lambda E = \int_E p d\alpha, \quad \text{and} \quad \lambda_n E = \int_E p_n d\alpha.$$

Moreover, for every α -measure set E , $\lim_{n \rightarrow \infty} \|p_n - p\|_1 = 0$. This implies that

$$\lim_{n \rightarrow \infty} p_n = p, \quad \text{in measure.}$$

Proof. To see this, notice that by equation (39) $p_n \rightarrow p$ in the normed space $L^1(\alpha)$. Let $\epsilon > 0$ and define measure sets $F_n = \{z \in \mathbb{C} \mid |p_n(z) - p(z)| > \epsilon\}$. Then

$$\int |p_n - p| d\alpha \geq \int_{F_n} |p_n - p| d\alpha \geq \epsilon \alpha F_n.$$

This shows that $\lim_{n \rightarrow \infty} \alpha F_n = 0$ and so $\lim_{n \rightarrow \infty} p_n = p$ in measure. \square

By the Lebesgue Dominated Convergence theorem for sequences which converge in measure it follows that for any α -measure set E , since $p_n \rightarrow p$ in measure,

$$\lambda E = \lim_{n \rightarrow \infty} \lambda_n E = \lim_{n \rightarrow \infty} \int_E p_n d\alpha = \int_E p d\alpha. \quad (40)$$

Since λ and λ_n are finite measures, and α is σ -finite, the Lebesgue Dominated Convergence theorem for sequences which converge in measure may be applied to the function $\varrho(a)$ in equation (23). That is, for any $a > 0$ on the positive real axis,

$$\begin{aligned} \varrho(a) &= \lim_{n \rightarrow \infty} \frac{1}{n} \sum_{j=1}^n \log(a - a_j) \\ &= \lim_{n \rightarrow \infty} \int_{\mathbb{C}} \log(a - z) d\lambda_n(z) \\ &= \lim_{n \rightarrow \infty} \int_{\mathbb{C}} \log(a - z) p_n(z) d\alpha(z) \\ &= \int_{\mathbb{C}} \log(a - z) p(z) d\alpha(z) = \int_{\mathbb{C}} \log(a - z) d\lambda(z). \end{aligned} \quad (41)$$

In other words, in terms of plane measure α and the limiting probability distribution function $p(z)$,

$$\varrho(a) = \int_E \log(a - z) p(z) d\alpha(z), \quad (42)$$

where the integration is over the entire complex plane with real plane measure α . Notice that for any α -measure set E , it similarly follows that

$$\lim_{n \rightarrow \infty} \frac{1}{n} \sum_{a_j \in E} \log(a - a_j) = \int_E \log(a - z) p(z) d\alpha(z). \quad (43)$$

This shows that the distribution $p(z)$ is unique up to zero α -measure sets.

Since $C = c_n^{(d-1)}$, the following theorem follows from equations (23) and (42).

Theorem 2.7. *Suppose that the partition function $A_n^+(a)$ of adsorbing walks of length n has a -plane zeros denoted by $\langle a_j \rangle$.*

In addition, suppose that $h_n(a)$ is a family of distribution functions on \mathbb{C} such that $h_n(a) \rightarrow 0$ if $|a| > 0$ and $n \rightarrow \infty$ and suppose that α is plane measure on \mathbb{C} . Then the set-function

$$\lambda_n E = \frac{1}{n} \int_E \sum_{j=1}^n h_{j,n}(a) d\alpha(a)$$

where $h_{j,n}(a) = h_n(a - a_j)$ is a probability measure on the σ -algebra of plane measure sets in \mathbb{C} .

Moreover, if the limit $\lambda E = \lim_{n \rightarrow \infty} \lambda_n E$ exists, then there exists a distribution function $p(z)$ on \mathbb{C} , unique up to zero α -measure sets, such that the limiting free energy of adsorbing walks is given by

$$\mathcal{A}^+(a) = \log \mu_{d-1} + \varrho(a) = \log \mu_{d-1} + \int_{\mathbb{C}} \log(a - z) p(z) d\alpha(z),$$

where $a \in \mathbb{R}^+$ (the positive real axis). □

The function $\mathcal{A}^+(a)$ can be analytically continued up to natural boundaries in the a -plane. Since $\mathcal{A}^+(a) = \log \mu_d$ if $a \in (0, a_c^+]$, it follows that $\varrho(a) = \log \frac{\mu_d}{\mu_{d-1}}$ for $a \in (0, a_c^+]$. In addition, $\varrho(a) \simeq \log a$ if $a \in \mathbb{R}$ and $a \rightarrow \infty$. Numerical approximations of $\varrho(a)$ may be made by approximating the distribution of zeros in the complex plane using the distribution functions h_n (or the distribution functions f_n and g_n in equations (28) and (30)). This gives numerical approximations to $\varrho(a)$ by $\frac{1}{n} \sum_{j=1}^n \log(a - a_j)$.

The function $\varrho(a)$ is singular at $a = a_c^+$ on the real axis. This shows that in the limit $n \rightarrow \infty$, a singular point develops on the real axis – this is the edge singularity.

In the limit as $a \rightarrow \infty$, $\log(a - z) = \log a - \frac{z}{a} + O(a^{-2})$. This gives

$$\mathcal{A}^+(a) = \log \mu_{d-1} + \log a - \frac{1}{a} \int_{\mathbb{C}} z p(z) d\alpha(z) + O(a^{-2}), \quad (44)$$

showing that $\mathcal{A}^+(a)$ is asymptotic to $\log \mu_{d-1} + \log a$ as $a \rightarrow \infty$.

Numerical approximations to the distribution $p_n(z)$ is obtained from equation (26). That is,

$$p_n(z) = \frac{1}{n} \sum_{j=1}^n h_{j,n}(z). \quad (45)$$

In this event, one may use the distribution functions $f_{j,n}(z)$ or $g_{j,n}(z)$ as examples. In the limit as $n \rightarrow \infty$, $p_n(a)$ is an approximation of the limiting distribution $p(z)$.

2.3.2. Radial and angular distribution of Fisher zeros: The radial and angular distribution of partition function zeros $\langle a_j \rangle$ can be considered in view of theorems 2.1 and 2.3. Define $\nu_n(\rho)$ and $\alpha_n(\theta, \phi)$ similar to the definitions in equation (15), but now for the zeros of $A_n^+(a)$. Proceed by computing L_n in theorem 2.1. By equation (7),

$$\begin{aligned} L_n &= \log \sum_{v=0}^n c_n^+(v) - \frac{1}{2} \log c_n^+(0) - \frac{1}{2} \log c_n^+(n) \\ &= \log c_n^+ - \frac{1}{2} \log c_{n-1}^+ - \frac{1}{2} \log c_n^{(d-1)} = \log \frac{c_n^+}{\sqrt{c_{n-1}^+ c_n^{(d-1)}}}, \end{aligned} \quad (46)$$

since $c_n^+(n) = c_n^{(d-1)}$. Dividing by n and taking $n \rightarrow \infty$ gives the result

$$\zeta_d = \lim_{n \rightarrow \infty} \frac{2}{n} L_n = \log \frac{\mu_d}{\mu_{d-1}}, \quad (47)$$

where $\mu_1 = 1$ (since $c_n^+(n) = 2$ if $n > 0$ in \mathbb{L}_+^2).

Observe that as $d \rightarrow \infty$, then the right hand side approaches zero. Otherwise, for $d = 2$, $\zeta_2 = \lim_{n \rightarrow \infty} \frac{2}{n} L_n \approx 0.970 < 1$ and for $d = 3$, $\zeta_3 = \lim_{n \rightarrow \infty} \frac{2}{n} L_n \approx 0.574 < 1$.

By theorem 2.1,

$$1 - \frac{2}{n\rho} L_n \leq \frac{1}{n} \nu_n(\rho) \leq 1. \quad (48)$$

That is, a positive fraction of the zeros are confined to the annulus $1 - \rho \leq |a| \leq \frac{1}{1 - \rho}$ in the a -plane if the left hand side is positive. Taking $n \rightarrow \infty$ gives

$$1 - \frac{1}{\rho} \zeta_d \leq \liminf_{n \rightarrow \infty} \frac{1}{n} \nu_n(\rho) \leq \limsup_{n \rightarrow \infty} \frac{1}{n} \nu_n(\rho) \leq 1. \quad (49)$$

The left hand side is positive if $\rho > \zeta_d$, and for these values of ρ there is a positive density of zeros in the annulus $1 - \rho \leq |a| \leq \frac{1}{1 - \rho}$.

Since $\liminf_{n \rightarrow \infty} \frac{1}{n} \nu_n(\rho) > 0$ if $\rho > \zeta_d$, this gives an upper bound on the critical point a_c^+ , namely $a_c^+ \leq \frac{1}{1-\zeta_d}$. This is a very poor bound in the square lattice, namely $a_c^+ \leq 33.42\dots$, since $\zeta_2 = \log 2.63815\dots = 0.97008\dots$ [10]. A slightly better bound is obtained in the cubic lattice, namely $a_c^+ \leq \log \frac{4.68404\dots}{2.63815\dots} = 2.347\dots$ [8, 10]. Numerical estimates of a_c^+ are $1.77564\dots$ in \mathbb{L}_+^2 [2] and $a_c^+ = 1.306 \pm 0.007$ in \mathbb{L}_+^3 [24]. In the limit $d \rightarrow \infty$ a positive fraction of the zeros accumulate on the unit circle in the a -plane.

Theorem 2.8. *Let $\zeta_d = \log \frac{\mu_d}{\mu_{d-1}}$ (and define $\mu_1 = 1$). If $\zeta_d < \rho < 1$, then*

$$0 < 1 - \frac{1}{\rho} \zeta_d \leq \liminf_{n \rightarrow \infty} \frac{1}{n} \nu_n(\rho) \leq \limsup_{n \rightarrow \infty} \frac{1}{n} \nu_n(\rho) \leq 1$$

and a positive fraction of partition function zeros of $A_n^+(a)$ are in the annulus $1-\rho < |a| < \frac{1}{1-\rho}$ in the complex a -plane. \square

The angular distribution of partition function zeros can be constrained by the Erdős-Turán theorem to

$$\left| \frac{1}{n} \alpha_n(\theta, \phi) - \frac{1}{2\pi} (\phi - \theta) \right|^2 \leq \frac{C_0}{n} L_n, \quad (50)$$

with L_n given in equation (46), and C_0 is an unknown constant. This shows, in particular, that

$$\frac{1}{2\pi} (\phi - \theta) - \sqrt{\frac{1}{n} C_0 L_n} \leq \frac{1}{n} \alpha_n(\theta, \phi) \leq \frac{1}{2\pi} (\phi - \theta) + \sqrt{\frac{1}{n} C_0 L_n}. \quad (51)$$

Taking $n \rightarrow \infty$ shows that

$$\begin{aligned} \frac{1}{2\pi} (\phi - \theta) - \sqrt{\frac{1}{2} C_0 \zeta_d} &\leq \liminf_{n \rightarrow \infty} \frac{1}{n} \alpha_n(\theta, \phi) \\ &\leq \limsup_{n \rightarrow \infty} \frac{1}{n} \alpha_n(\theta, \phi) \leq \frac{1}{2\pi} (\phi - \theta) + \sqrt{\frac{1}{2} C_0 \zeta_d}. \end{aligned} \quad (52)$$

Theorem 2.9. *Let $\zeta_d = \log \frac{\mu_d}{\mu_{d-1}}$. If $\zeta_d < \rho < 1$, then there exists a constant C_0 such that*

$$\limsup_{n \rightarrow \infty} \left| \frac{1}{n} \alpha_n(\theta, \phi) - \frac{1}{2\pi} (\phi - \theta) \right| \leq \sqrt{\frac{1}{2} C_0 \zeta_d}. \quad \square$$

In low dimensions this is not a strong result, but in the limit as $d \rightarrow \infty$, $\zeta_d \rightarrow 0$. That is, if $C_0 \zeta_d \rightarrow 0$ as $d \rightarrow \infty$, then $\limsup_{n \rightarrow \infty} \left| \frac{1}{n} \alpha_n(\theta, \phi) - \frac{1}{2\pi} (\phi - \theta) \right| \rightarrow 0$. This does not prove, but does suggest that the angular distribution of zeros may become more uniform in higher dimensions.

Since $\limsup_{n \rightarrow \infty} \frac{1}{n} \alpha_n(-\pi, \phi)$ is a monotonic function of ϕ , it is measurable and differentiable almost everywhere in $(-\pi, \pi]$. This shows that there exists a measurable function q such that

$$\limsup_{n \rightarrow \infty} \frac{1}{n} \alpha_n(-\pi, \phi) = \int_{-\pi}^{\phi} q(\psi) d\psi, \quad (53)$$

where the integral is the Lebesgue integral. The function q is a distribution function, and

$$\int_{[\theta, \phi]} dq = \int_{\theta}^{\phi} q(\psi) d\psi \quad (54)$$

is the fraction of zeros with principal argument greater than or equal to θ and less than or equal to ϕ .

The bounds on the distribution of zeros above (obtained by using theorem 2.3, the Erdős and Turán theorem) may be slightly improved by using the theorem of Erdélyi [11]. As before, let $P(t)$ be a polynomial with zeros $\langle t_1, t_2, \dots, t_N \rangle$. Define the following functions related to $\alpha_N(\theta, \phi)$:

$$\begin{aligned}\alpha_N^+(\theta, \phi) &= \# \{t_k | \theta < \Re t_k \leq \phi, \text{ and } |t_k| \geq 1\}; \\ \alpha_N^-(\theta, \phi) &= \# \{t_k | \theta < \Re t_k \leq \phi, \text{ and } |t_k| \leq 1\}.\end{aligned}\quad (55)$$

Theorem 2.10 (Erdélyi [11]). *Suppose $\langle a_n \rangle$ is a sequence in \mathbb{C} and suppose that $|a_0 a_N| \neq 0$. Define $P(t) = \sum_{n=0}^N a_n t^n$ and let $\|P\| = \max_{|t|=1} \{|P(t)|\}$. Then*

$$\frac{1}{N} \alpha_N^+(\theta, \phi) - \frac{1}{2\pi} (\phi - \theta) \leq 16 \sqrt{\frac{1}{N} \log R_1};$$

and

$$\frac{1}{N} \alpha_N^-(\theta, \phi) - \frac{1}{2\pi} (\phi - \theta) \leq 16 \sqrt{\frac{1}{N} \log R_2},$$

where

$$R_1 = |a_N|^{-1} \|P\|, \text{ and } R_2 = |a_0|^{-1} \|P\|.$$

□

In the particular case here, the polynomial $P(t)$ is the partition function $A_n^+(a)$. It follows that $\log R_1 = \log \frac{c_n^+}{c_n^{(d-1)}}$ and $\log R_2 = \log \frac{c_n^+}{c_{n-1}^+}$. Notice that

$$\lim_{n \rightarrow \infty} \frac{1}{n} \log R_1 = \log \frac{\mu_d}{\mu_{d-1}}.$$

Since $c_{n-1}^+ \leq c_n^+ \leq 2d c_{n-1}^+$ it follows that $1 \leq \limsup_{n \rightarrow \infty} \log \frac{c_n^+}{c_{n-1}^+} \leq \log 2d$. In other words,

$$\frac{1}{n} \log R_2 = O\left(\frac{1}{n}\right).$$

Put these results together in theorem 2.10 to obtain

$$\frac{1}{n} \alpha_n^+(\theta, \phi) - \frac{1}{2\pi} (\phi - \theta) \leq 16 \sqrt{\frac{1}{n} \log \frac{c_n^+}{c_n^{(d-1)}}} = O(1) \quad \text{as } n \rightarrow \infty;$$

and

$$\frac{1}{n} \alpha_n^-(\theta, \phi) - \frac{1}{2\pi} (\phi - \theta) \leq 16 \sqrt{\frac{1}{n} \log \frac{c_n^+}{c_{n-1}^+}} = O\left(\frac{1}{\sqrt{n}}\right) \rightarrow 0 \quad \text{as } n \rightarrow \infty.$$

These results give a slightly better outcome, since the bounds are numerical, not involving a constant C_0 of unknown magnitude as in corollary 2.9.

In the limit as $n \rightarrow \infty$,

$$\limsup_{n \rightarrow \infty} \frac{1}{n} \alpha_n^-(\theta, \phi) \leq \frac{1}{2\pi} (\phi - \theta). \quad (56)$$

Notice that

$$\lim_{\theta \nearrow \phi} \alpha_n^-(\theta, \phi) = O(\sqrt{n}). \quad (57)$$

In other words, as n increases, the multiplicity of Fisher zeros with $|a| \leq 1$ will increase at a rate no faster than $O(\sqrt{n})$.

Adding the contributions from α_n^- and α_n^+ show that, given a small $\epsilon > 0$, there exists an N such that

$$\frac{1}{n}\alpha_n(\theta, \phi) \leq \frac{1}{n}\alpha_n^-(\theta, \phi) + \frac{1}{n}\alpha_n^+(\theta, \phi) \leq \frac{1}{\pi}(\phi - \theta) + 16\sqrt{\log \frac{\mu_d}{\mu_{d-1}}} + \epsilon. \quad (58)$$

for all $n \geq N$. This is an improvement on equation (51) in that there are no arbitrary constants C_0 involved. However, this bound is not very useful in low dimensions, but since the square root term approaches zero with increasing d , it gives a useful bound in high dimensions.

Taking the limsup on the left hand side as $n \rightarrow \infty$ gives

$$\limsup_{n \rightarrow \infty} \frac{1}{n}\alpha_n(\theta, \phi) \leq \frac{1}{\pi}(\phi - \theta) + 16\sqrt{\log \frac{\mu_d}{\mu_{d-1}}}. \quad (59)$$

This gives the following theorem:

Theorem 2.11. *Let $\alpha_n(\theta, \phi)$ be the number of Fisher zeros with principal argument in $[\theta, \phi]$ in the complex a -plane. Then there exists a measurable function q defined by*

$$\int_{\theta}^{\phi} q(\psi) d\psi = \limsup_{n \rightarrow \infty} \frac{1}{n}\alpha_n(\theta, \phi),$$

where $-\pi < \theta \leq \phi \leq \pi$. The function q is the distribution function of the principal arguments of the zeros of $A_n^+(a)$ in the limit as $n \rightarrow \infty$. Moreover,

$$\int_{[\theta, \phi]} dq = \int_{\theta}^{\phi} q(\psi) d\psi \leq \min\left\{\frac{1}{\pi}(\phi - \theta) + 16\sqrt{\log \frac{\mu_d}{\mu_{d-1}}}, 1\right\},$$

where the integral is the Lebesgue integral on $[-\pi, \pi]$. □

2.4. Yang-Lee zeros

Lee-Yang zeros were defined in section 2.2 as t -plane zeros of the partial generating function $G_N(a, t)$ (see equation (14)). In this section the a -plane zeros of $G_N(a, t)$ are considered; these will be called *Yang-Lee zeros*. Generally, since for fixed values of t the partial sum $G_N(a, t)$ is a linear combination of the partition functions $A_n^+(a)$, the Yang-Lee zeros will have properties similar to the properties of partition function (or Fisher) zeros.

Define

$$B_v(t) = \sum_{n=v}^N c_n^+(v) t^n. \quad (60)$$

Then the partial sums of the generating function are

$$G_N(a, t) = \sum_{n=0}^N A_n^+(a) t^n = \sum_{v=0}^N \sum_{n=v}^N c_n^+(v) t^n a^v = \sum_{v=0}^N B_v(t) a^v. \quad (61)$$

In the context here, the function $\nu_N(\rho)$ (see equation (15)) is the number of a -plane zeros of $G_N(a, t)$ in the annulus $1 - \rho \leq |a| \leq \frac{1}{1 - \rho}$. To apply theorem 2.1, compute L_N :

$$L_N = \log \sum_{v=0}^N B_v(t) - \frac{1}{2} \log B_N(t) - \frac{1}{2} \log B_0(t)$$

$$\begin{aligned}
&= \log \sum_{n=0}^N \sum_{v=0}^n c_n^+(v) t^n - \frac{1}{2} \log c_N^+(N) t^N - \frac{1}{2} \log \sum_{n=0}^N c_n^+(0) t^n \\
&= \log \sum_{n=0}^N c_n^+ t^n - \frac{1}{2} \log c_N^{(d-1)} t^N - \frac{1}{2} \log \sum_{n=1}^N c_{n-1}^+ t^n \\
&= \log \sum_{n=0}^N c_n^+ t^n - \frac{1}{2} \log c_N^{(d-1)} t^N - \frac{1}{2} \log \sum_{n=0}^{N-1} c_n^+ t^n - \frac{1}{2} \log t \\
&= \log \left[\frac{\sum_{n=0}^N c_n^+ t^n}{(\sum_{n=0}^{N-1} c_n^+ t^n)^{1/2} (c_N^{(d-1)} t^N)^{1/2}} \right] - \frac{1}{2} \log t. \tag{62}
\end{aligned}$$

Suppose that t is large, so that $c_n^+ t^n = (\mu_d t)^{n+o(n)} \rightarrow \infty$ as $n \rightarrow \infty$ (that is, $t > \frac{1}{\mu_d}$). Then the summations above are dominated by their fastest exponentially growing terms, and the result is that (see equation (47))

$$\lim_{N \rightarrow \infty} \frac{2}{N} L_N = \log \frac{\mu_d}{\mu_{d-1}} = \zeta_d. \tag{63}$$

By theorem 2.1, this is similar to equation (48), namely, for finite n and $\rho \in (0, 1)$

$$1 - \frac{2}{N\rho} L_n \leq \frac{1}{N} \nu_N(\rho) \leq 1 + \frac{2}{N\rho} L_n. \tag{64}$$

Since $\nu_N(\rho) \leq N$, the result is that, in the limit $N \rightarrow \infty$,

$$1 - \frac{1}{\rho} \zeta_d \leq \liminf_{N \rightarrow \infty} \frac{1}{N} \nu_N(\rho) \leq \limsup_{N \rightarrow \infty} \frac{1}{N} \nu_N(\rho) \leq 1, \tag{65}$$

where $\zeta_d = \log \frac{\mu_d}{\mu_{d-1}}$. This result is similar to theorem 2.8, namely that for $\zeta_d < \rho < 1$, a positive fraction of the Yang-Lee zeros are confined to the annulus $1 - \rho \leq |a| \leq \frac{1}{1-\rho}$ in the a -plane. This gives the following theorem:

Theorem 2.12. Suppose that $t > \frac{1}{\mu_d}$. Define $\zeta_d = \log \frac{\mu_d}{\mu_{d-1}}$ (where $\mu_1 = 1$). If $\zeta_d < \rho < 1$, then

$$0 < 1 - \frac{1}{\rho} \zeta_d \leq \liminf_{N \rightarrow \infty} \frac{1}{N} \nu_N(\rho) \leq \limsup_{N \rightarrow \infty} \frac{1}{N} \nu_N(\rho) \leq 1$$

and a positive fraction of Yang-Lee zeros of $G_N^+(a, t)$ are in the annulus $1 - \rho < |a| < \frac{1}{1-\rho}$ in the complex a -plane. \square

Consider next the case that t is small, namely $t < \frac{1}{\mu_d} < \frac{1}{\mu_{d-1}}$. Then there is a constant K such that $c_n^+ t^n \leq K$ for all $n \in \mathbb{N}$. In particular, $1 \leq \sum_{n=0}^N c_n^+ t^n \leq K(N+1)$. This shows that $\lim_{N \rightarrow \infty} (\sum_{n=0}^N c_n^+ t^n)^{1/N} = 1$. Thus, by equation (62),

$$\xi_t = \lim_{N \rightarrow \infty} \frac{2}{N} L_N = -\log(\mu_{d-1} t) > 0 \tag{66}$$

since $t < \frac{1}{\mu_{d-1}}$.

Observe that $\xi_t < 1$ if $t \in (\frac{1}{e\mu_{d-1}}, \frac{1}{\mu_d})$ and if $\mu_d < e\mu_{d-1}$. In \mathbb{L}_+^2 this gives the range $t \in (0.36787\dots, 0.37905\dots)$, and in \mathbb{L}_+^3 , $t \in (0.13944\dots, 0.21349\dots)$. For these values t , $\xi_t < 1$ and there is a $\rho \in (\xi_t, 1)$ for which a positive fraction of zeros are confined in an annulus $1 - \rho < |a| < \frac{1}{1-\rho}$ in the complex a -plane. This gives the theorem:

Theorem 2.13. Suppose that $t \in (\frac{1}{e\mu_{d-1}}, \frac{1}{\mu_d})$. Define $\xi_t = |\log(\mu_{d-1}t)|$ (where $\mu_1 = 1$). If $\xi_t < \rho < 1$, then

$$0 < 1 - \frac{1}{\rho} \xi_t \leq \liminf_{N \rightarrow \infty} \frac{1}{N} \nu_N(\rho) \leq \limsup_{N \rightarrow \infty} \frac{1}{N} \nu_N(\rho) \leq 1$$

and a positive fraction of Yang-Lee zeros of $G_N^+(a, t)$ are in the annulus $1 - \rho < |a| < \frac{1}{1-\rho}$ in the complex a -plane. \square

Theorems 2.12 and 2.13 do not rule out the possibility that zeros may accumulate in an annular region for $0 < t \leq \frac{1}{e\mu_{d-1}}$.

The angular distribution of Yang-Lee zeros can be considered using theorem 2.10. In this case, the polynomial is $G_N(a, t) = \sum_{v=0}^N B_v(t) a^v$ (equation (61)). Similar to the above, let $\alpha_N(\theta, \phi)$ be defined as in equation (15), but now for Yang-Lee zeros of the partial generating function $G_N(a, t)$ in the a -plane. Proceed by computing R_1 and R_2 in theorem 2.10: First, notice that

$$\|G_N(a, t)\| = \max_{|a|=1} \left\{ \sum_{v=0}^N B_v(t) a^v \right\} = \sum_{v=0}^N B_v(t) = \sum_{v=0}^N \sum_{n=v}^N c_n^+(v) t^n = \sum_{n=0}^N c_n^+ t^n.$$

This gives for R_1 :

$$R_1 = B_N(t)^{-1} \|G_N(a, t)\| = \frac{\sum_{n=0}^N c_n^+ t^n}{c_N^+ t^N} = \frac{\sum_{n=0}^N c_n^+ t^n}{c_N^{(d-1)} t^N}. \quad (67)$$

Taking logs, dividing by N , and taking $N \rightarrow \infty$, shows that

$$\lim_{N \rightarrow \infty} \frac{1}{N} \log R_1 = \begin{cases} \log \frac{\mu_d}{\mu_{d-1}}, & \text{if } t > \frac{1}{\mu_d}; \\ -\log(\mu_{d-1}t) & \text{if } t \leq \frac{1}{\mu_d}. \end{cases} \quad (68)$$

R_2 is computed in a similar way, namely

$$R_2 = B_0(t)^{-1} \|G_N(a, t)\| = \frac{\sum_{n=0}^N c_n^+ t^n}{c_N^+ t^N}. \quad (69)$$

Taking logs, dividing by N , and taking $N \rightarrow \infty$, shows that

$$\lim_{N \rightarrow \infty} \frac{1}{N} \log R_2 = 0, \quad (70)$$

for all $t > 0$, since the numerator and denominator grows at the same exponential rate in equation (69) if $t > \frac{1}{\mu_d}$. Since the result in equation (68) is positive for almost all $t > 0$, it follows by theorem 2.10 that

$$\begin{aligned} \limsup_{N \rightarrow \infty} \frac{1}{N} \alpha_N^+(\theta, \phi) - \frac{1}{2\pi} (\phi - \theta) &\leq 16 \begin{cases} \sqrt{\log \frac{\mu_d}{\mu_{d-1}}}, & \text{if } t > \frac{1}{\mu_d}; \\ \sqrt{|\log(\mu_{d-1}t)|}, & \text{if } t \leq \frac{1}{\mu_d}. \end{cases} \quad (71) \\ \limsup_{N \rightarrow \infty} \frac{1}{N} \alpha_N^-(\theta, \phi) - \frac{1}{2\pi} (\phi - \theta) &\leq 0. \end{aligned}$$

Adding these results give

$$\limsup_{N \rightarrow \infty} \frac{1}{N} \alpha_N(\theta, \phi) \leq \frac{1}{\pi} (\phi - \theta) + 16 \begin{cases} \sqrt{\log \frac{\mu_d}{\mu_{d-1}}}, & \text{if } t > \frac{1}{\mu_d}; \\ \sqrt{|\log(\mu_{d-1}t)|}, & \text{if } t \leq \frac{1}{\mu_d}. \end{cases} \quad (72)$$

This is not a particularly good bound on the limsup, since the factor of 16 is quite significant. It is also the case that $\lim_{N \rightarrow \infty} \frac{1}{N} \alpha_N(\theta, \phi) \leq 1$, and since $16\sqrt{\log \mu_2} \approx 15.76$

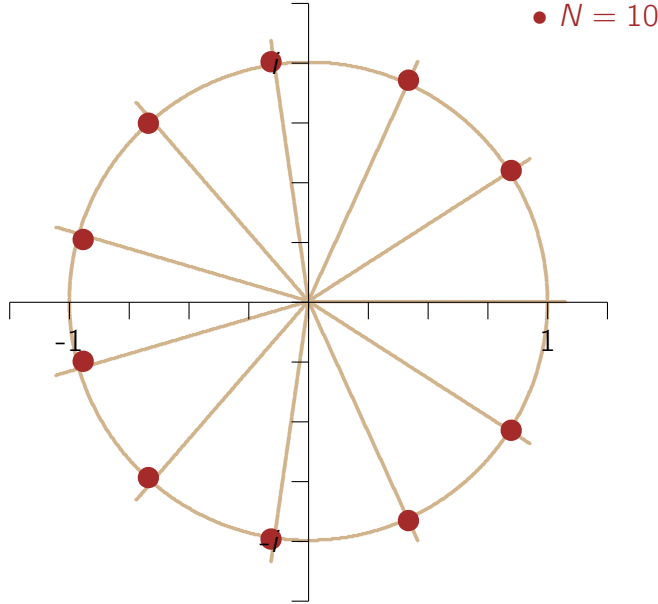


Figure 2: Approximate locations of the zeros of $g_N(a, t)$ for $N = 10$ and $a = 1$. The zeros are approximately on the unit circle, and close to ten vertices of a regular 11-gon with centre at the origin (and with one corner placed at the point $(1, 0)$, as illustrated). The rays from the origin are the spokes of the regular 11-gon. The least squares ellipse through the points has approximate centre $(0.011, 0)$, approximate half short axis of length 1.00, and approximate half long axis of length 1.01.

and $16\sqrt{\log \frac{\mu_3}{\mu_2}} \approx 12.12$, this bound is not useful in \mathbb{L}_+^d if $d = 2$ or $d = 3$. However, taking d large has the consequence that $\sqrt{\log \frac{\mu_d}{\mu_{d-1}}} \rightarrow 0$, so that the bound becomes far better, and approaches the bound given in equation (56) for Fisher zeros.

Similar to the case for Fisher zeros, there exists an angular distribution function $s(\psi)$ for Yang-Lee zeros. This distribution function is similarly constrained by the results above in high dimensions, as shown in the following theorem:

Theorem 2.14. *Let $\alpha_N(\theta, \phi)$ be the number of Yang-Lee zeros with principal argument in $[\theta, \phi]$ in the complex a -plane. Suppose that s is defined by*

$$\int_{\theta}^{\phi} s(\psi) d\psi = \limsup_{n \rightarrow \infty} \frac{1}{N} \alpha_N(\theta, \phi),$$

where $-\pi < \theta \leq \phi \leq \pi$. Then s is a distribution function of the principal arguments of the a -plane zeros of $G_N(a, t)$ in the limit as $n \rightarrow \infty$. Moreover, if $t > \frac{1}{\mu_d}$, then

$$\int_{[\theta, \phi]} ds = \int_{\theta}^{\phi} s(\psi) d\psi \leq \min\left\{\frac{1}{\pi}(\phi - \theta) + 16\sqrt{\log \frac{\mu_d}{\mu_{d-1}}}, 1\right\},$$

where the integral is the Lebesgue integral on $[-\pi, \pi]$.

Similarly, if $t < \frac{1}{\mu_d}$, then

$$\int_{[\theta, \phi]} ds = \int_{\theta}^{\phi} s(\psi) d\psi \leq \min\left\{\frac{1}{\pi}(\phi - \theta) + 16\sqrt{|\log(\mu_{d-1}t)|}, 1\right\}. \quad \square$$

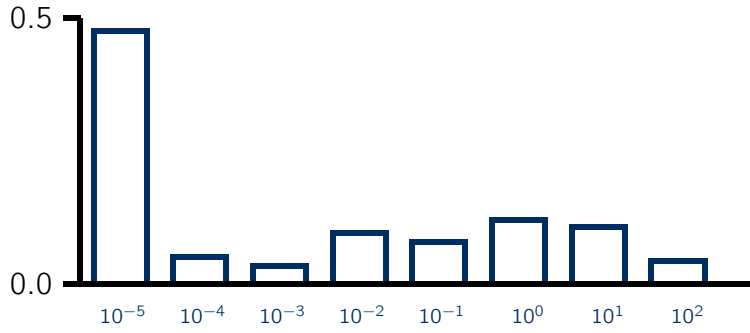


Figure 3: A histogram showing the distribution of $|c_n^+(k)(a_j^*)^k|/|A_n^+(a_j)|$ for $n = 400$ in the half square lattice. Bars with label 10^{-n} represent the fraction of ratios of size larger than 10^{-n-1} and smaller or equal to 10^{-n} . Almost all the ratios are smaller than 10^{-5} , and less than 10% of the ratios are bigger than 1. The sizes of those ratios exceeding 1 are still well smaller than 10^2 .

3. Numerical determination of the distribution of zeros

In this section the location and distribution of Fisher zeros are examined, using in particular the measures μ_n and ν_n in equations (29) and (31). Similar comments can be made about Lee-Yang zeros, but since these are, from a numerical point of view, very stably distributed along a circle in the t -plane, it appears that numerical error is not a concern here. For example, the zeros of $g_N(a, t)$ for $N = 10$ and $a = 1$ are shown in figure 2. These are located very close to the vertices of a 11-gon on the unit circle in the t -plane (with no zero close to the vertex on the positive real axis). Similar results will be presented in sections 4.1 and 5.1.

3.1. Numerical location of Fisher zeros

Numerical estimates of $c_n^+(\nu)$ in \mathbb{L}_+^2 and \mathbb{L}_+^3 were obtained by using the GAS algorithm [26] to approximately enumerate self-avoiding walks [22] in half lattices. In each case the algorithm was used to sample along 10^3 sequences each of length 10^9 iterations (see reference [24] for details), estimating microcanonical data for $0 \leq \nu \leq n$ where $0 \leq n \leq 500$ over 10^{12} iterations. Since the algorithm estimates approximate values $\bar{c}_n^+(\nu)$ for $c_n^+(\nu)$, the numerically determined partition functions and partial generating functions are only approximations to $A_n^+(a)$ and $G_N(a, t)$ in \mathbb{L}_+^2 and \mathbb{L}_+^3 .

An error in the estimate of $c_n^+(\nu)$ will change the locations of partition and partial generating function zeros. The degree to which this is the case may be examined by assuming a small relative error of ϵ in one of the estimates (so that $\bar{c}_n^+(\nu) = (1+\epsilon)c_n^+(\nu)$), and then to examine the impact this has on the locations of zeros.

Consider the partition function $A_n^+(a)$ and suppose that the coefficient of a^k has a small relative error (that is, $\bar{c}_n^+(k) = (1+\epsilon)c_n^+(k)$). Define the perturbed partition function $P_n(a)$ by

$$P_n(a) = A_n^+(a) + \epsilon c_n^+(k) a^k. \quad (73)$$

Suppose that the j -th zero of $A_n^+(a)$ is a_j , and that the zeros of $P_n(a)$ are denoted by $\langle a_j^* \rangle$. Then there is a labeling of the zeros so that $a_j^* = a_j$ for each j if $\epsilon = 0$. If $|\epsilon| > 0$

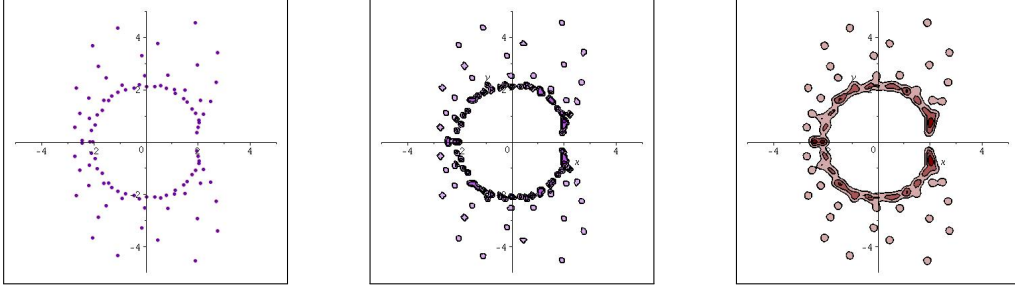


Figure 4: Left: Fisher zeros for $n = 100$ in $d = 2$ dimensions. The distribution of zeros can be estimated from this data using the measures μ_n and ν_n . Middle: The distribution of Fisher zeros using the measure μ_n and the data on the Left. Right: The distribution using the measure ν_n and the data on the Left.

is very small, then assume that for the j -th zero, $a_j^* = a_j + \delta_j$ for some value of δ_j . The size of δ_j will be estimated as follows: Consider

$$\begin{aligned} P_n(a_j^*) &= A_n^+(a_j^*) + \epsilon c_n^+(k)(a_j^*)^k \\ &= A_n^+(a_j) + \delta_j A_n^{+'}(a_j) + O(\delta_j^2) + \epsilon c_n^+(k)(a_j^*)^k, \end{aligned}$$

where it is assumed that $A_n^{+'}(a_j) \neq 0$. Since $P_n(a_j^*) = A_n^+(a_j) = 0$, solve for δ_j to leading order in ϵ :

$$\delta_j = \frac{\epsilon c_n^+(k)(a_j^*)^k}{A_n^{+'}(a_j)} + O(\epsilon^2). \quad (74)$$

This shows that $\delta_j \rightarrow 0$ as $\epsilon \rightarrow 0$. Since the relative error ϵ approaches zero as the GAS algorithm continues to run; it follows that δ_j decreases in size with the length of the simulation, and the estimates of locations of zeros improve.

It is not possible to estimate ϵ in the above, except in some cases where $c_n^+(k)$ is known. For example, $c_n^+(n) = 2$ in the half square lattice for all $n > 0$. The GAS algorithm in our simulations converged to $c_{400}^+(400) \approx 1.9772$, giving $|\epsilon| \lesssim 0.012$. Similarly, for $n = 500$ the result is $c_{500}^+(500) \approx 1.9751$, so that $|\epsilon| \lesssim 0.013$. Incidentally, these estimates show that the GAS algorithm samples well into the tails of the distribution $c_n^+(\nu)$ in (n, ν) , and its estimates of the microcanonical partition function in the tails of the distribution over state space is very good – this is an example of rare event sampling (and is a quality this algorithm shares with the PERM and flatPERM algorithms [16, 39]).

In three dimensions $c_n^+(n)$ is the number of square lattice walks. If $n = 50$ then the estimate obtained by the GAS algorithm is $c_{50}^+(50) \approx 5.29279 \times 10^{21}$ while exact enumeration [27] gives $c_{50}^+(50) = 5.30324 \dots \times 10^{21}$. This gives $|\epsilon| \lesssim 0.0020$. A similar comparison for $n = 70$ gives $\epsilon \lesssim 0.0050$.

For other values of n and ν the relative error ϵ can be estimated by dividing the standard error of the estimates by the estimate. That is, if the estimate $\bar{c}_n^+(\nu)$ has standard error $e_n^+(\nu)$, then ϵ is estimated by the ratio $e_n^+(\nu)/\bar{c}_n^+(\nu)$. This gives $\epsilon \lesssim 0.01$ consistently in \mathbb{L}_2^+ and \mathbb{L}_3^+ , for $n \leq 450$, and for $n > 450$ it grows to a couple of percent for a few values of ν (but otherwise remains well below 1%).

These results suggest that, generally, one may assume that $\epsilon \lesssim 0.01$ (or that the microcanonical data were estimated to a relative error of about 1% for most values of $0 \leq \nu \leq n$ and $n \leq 500$ and for most values of (n, ν) in fact far better than this).

The size of δ_j is also a function of the size of the ratios $|c_n^+(k)(a_j^*)^k|/|A_n^{+'}(a_j)|$. Summing equation (74) over k gives an estimate of the total contribution if ϵ is a fixed error on all the data. Since δ_j is a complex number, this gives the total estimated error

$$\Delta_j = \epsilon \frac{A_n^+(a_j^*)}{A_n^{+'}(a_j)} + O(n\epsilon^2). \quad (75)$$

Estimates of this quantity (with a_j replaced by a_j^* in our data) are always very small, and never exceeded 10^{-5} . However, this is very likely an underestimate of the error in the location of the a_j^* .

An alternative approach, which should give a large overestimate of the error, is to estimate $|c_n^+(k)(a_j^*)^k|/|A_n^{+'}(a_j)|$ and sum these contributions over k . The size distribution of $|c_n^+(k)(a_j^*)^k|/|A_n^{+'}(a_j)|$ is displayed for $n = 400$ in figure 3. Notice the logarithmic scale on the horizontal axis of the histogram. The height of each bar is proportional to the fraction of ratios which has size less than the power of 10 shown at the bottom of the bar. Summing the contributions give, in all cases, a result between 10 and 100 (and consistently well less than 100). Since this is the result if all the magnitudes of the errors are added up without cancellations, multiplying this by ϵ likely gives an overestimate of the error in the location of the a_j^* .

If one accepts that the contribution of the ratio $\frac{c_n^+(k)(a_j^*)^k}{A_n^{+'}(a_j)}$ to lie between 10^{-5} and 10^2 , and $\epsilon \lesssim 10^{-2}$, then δ_j will be very small for most values of j , and large for a few values of j . These results suggest that a few zeros will move quickly with uncertainties in the data, and equation (74) indicates that this will be particularly true for cases where $|a_j^*|$ is large. Most zeros, however, should be quite stable.

Similar observations apply to the a -plane zeros of the partial generating function $G_N(a, t)$.

3.2. The numerical distribution of Fisher zeros

The distribution of Fisher zeros were measured in section 2.3.1 using the probability measure λ_n . Two examples of measures were given in equations (29) and (31), namely the measures μ_n and ν_n . These measures give distributions functions p_n on the a -plane zeros. In this section this is considered from a numerical point of view, using the approximate enumeration data generated by the GAS algorithm.

In figure 4 the locations of approximate a -plane zeros of $A_n^+(a)$ for $n = 100$ and $d = 2$ is shown. On the left are the locations of the zeros, and in the middle and on the right are contour plots of the distribution p_n of zeros using the measures μ_n (with $\tau_n = n$; see equation (29)) and ν_n (with $\tau_n = \frac{1}{2}\sqrt{n}$; see equation (31)), respectively.

The stability of the distribution p_n (or its dependence on uncertainties in the numerical data), may be examined by tracking the distribution of the estimated zeros as the length of the simulation increases. The result is shown in figure 5 for p_n in the half square lattice. The first contour plot (top, left) is the distribution p_n , determined by using the measure ν_n (with $\tau_n = \frac{1}{2}\sqrt{n}$; see equation (31)). In this case the data were obtained by using the GAS algorithm to sample along 10 sequences, each of length 10^9 iterations.

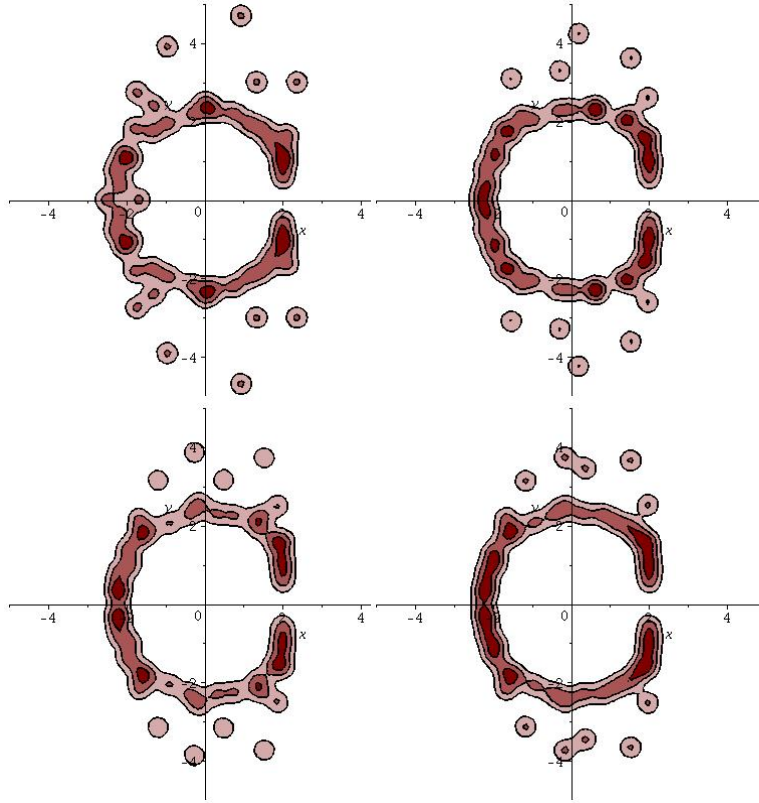


Figure 5: The evolution of the distribution p_n for a -plane zeros for $n = 50$ and sampling along M GAS-sequences of length 10^9 . Top Left: The distribution for $M = 10$ (10 sequences of length 10^9 each). Top Right: the distribution for $M = 100$. Bottom Left: $M = 250$, and Bottom Right: $M = 400$. These contour plots, computed by using the locations of the zeros and the measure ν_n , show remarkable consistency with increasing N as the zeros accumulate in a pattern on a circle of radius equal to the critical value of a (the critical adsorption point a_c^+) in the half square lattice. Notice the formation of the edge singularity on the positive real axis.

Increasing the length of the simulation to 100 sequences of length 10^9 gives the second contour plot (top, right). While the contours have changed, the distribution is still recognizable. Notice that those isolated zeros far from the origin moved from their locations. The distributions can be compared by computing the $L_1(\alpha)$ -norm (which has a maximum of 2) of the absolute difference between the distributions p_n for simulations of $N = 10$ and $N = 100$ sequences (and for walks of length $n = 50$). With respect to μ_n with $\tau_n = \frac{1}{9}n$ this gives 0.634 and with respect to ν_n with $\tau_n = \frac{1}{2}\sqrt{n}$, the $L_1(\alpha)$ -norm is 0.596.

Increasing the length of the simulation to 250 sequences of length 10^9 iterations gives the distribution on the bottom left. The contours changed, but the overall shape of the distribution remained similar. Computing the $L_1(\alpha)$ -norm of the absolute difference between the distributions at $N = 100$ and $N = 250$ gives 0.398 with respect to μ_n ($\tau_n = \frac{1}{9}n$) and 0.354 with respect to ν_n ($\tau_n = \frac{1}{2}\sqrt{n}$), respectively.

For $N = 400$ the distribution is given by the contour plot on the bottom right. The $L_1(\alpha)$ -norm of this distribution and the distribution at $N = 250$ is 0.195 with respect to μ_n and 0.181 with respect to ν_n , respectively. Letting the simulation run to $N = 1000$

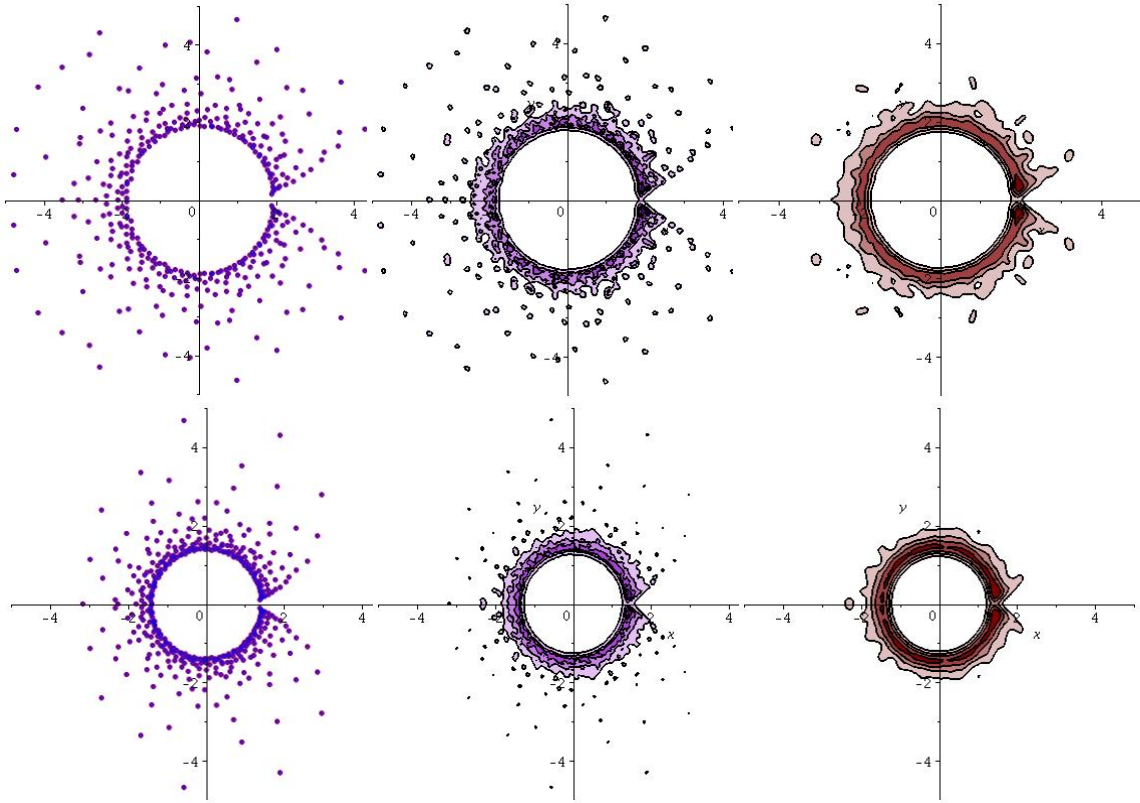


Figure 6: Fisher zeros of square lattice adsorbing walks of length $n = 400$ (top row), and of cubic lattice adsorbing walks of length $n = 400$ (bottom row). Top left is the locations of the calculated zeros, top middle a contour plot of the distribution of zeros computed from using the measure μ_n in equation (29) with $\tau_n = n$, and top right a contour plot of the distribution of zeros computed by using the measure ν_n with $\tau_n = \frac{1}{2}\sqrt{n}$ in equation (31). Along the bottom row the same plots are shown, but now for data for cubic lattice walks of length $n = 400$.

sequences each of length 10^9 gives the final distribution illustrated in figure 6 (in this case illustrated for $n = 400$). The formation of an edge-singularity on the positive real axis is seen as the leading zeros approach the positive real axis. In this figure the contour plots in the middle and on the right were determined using the measures μ_n with $\tau_n = n$, and ν_n with $\tau_n = \frac{1}{2}\sqrt{n}$ in equations (29) and (31) respectively.

The convergence of $p_n \rightarrow p$ as $n \rightarrow \infty$ can be tracked by computing the $L_1(\alpha)$ -norm of $(p_n - p)$ as a function of n (while taking $p \approx p_{500}$ as the best estimate of the limiting distribution). This is tabulated in table 1. Notice that increasing n decreases the $L_1(\alpha)$ -norm in each case, showing that the distribution p_n approaches p_{500} systematically with increasing n . This is strong supporting evidence that the distribution of zeros produced by the algorithm behave consistently with increasing n . Similar results are seen in \mathbb{L}_+^3 .

The relation between the distributions obtained from the μ_n and ν_n measures can also be examined by computing the $L_1(\alpha)$ -norm of the difference between the distributions. If $p_n(\mu_n)$ is the distribution obtained from the μ_n -measure, and $p_n(\nu_n)$ is the distribution obtained from the ν_n -measure, then $\|p_n(\mu_n) - p_n(\nu_n)\|_1 = 0.363$ if $n = 50$ and $\tau_n = \frac{n}{9}$ for μ_n and $\tau_n = \frac{1}{2}\sqrt{n}$ for ν_n . For $n = 500$, the distance is slightly larger at $\|p_n(\mu_n) - p_n(\nu_n)\|_1 = 0.517$.

Table 1: $\|p_n - p_{500}\|_1$ with respect to μ_n and ν_n in \mathbb{L}_+^2

n	$\ p_n - p_{500}\ _1$ wrt μ_n ($\tau_n = \frac{n}{9}$)	$\ p_n - p_{500}\ _1$ wrt ν_n ($\tau_n = \frac{1}{2}\sqrt{n}$)
50	1.113	1.028
100	0.948	0.775
200	0.869	0.581
300	0.813	0.595
350	0.756	0.427
400	0.735	0.399
420	0.678	0.363
440	0.723	0.390
460	0.700	0.373
470	0.689	0.379
480	0.659	0.345
490	0.648	0.339
495	0.537	0.288

4. Numerical Results in the Square Lattice

4.1. Lee-Yang zeros of $G_N(a, t)$ in the square lattice

The t -plane zeros of $G_N(a, t)$ are in general functions of a (and of N), but will be converging on the circle $|t| = \lambda_a^{-1}$ in the t -plane as $N \rightarrow \infty$ by theorem 2.2 (where λ_a is defined by equation (16)). Moreover, by theorem 2.4 the complex arguments of the zeros should approach a uniform distribution. That is, the t -plane zeros of $G_N(a, t)$ should be distributed, in the limit, uniformly on a circle of radius λ_a^{-1} .

To investigate the above numerically, approximate λ_a by

$$\lambda_a(N) = (A_N^+(a))^{1/N}. \quad (76)$$

In particular, $\lim_{N \rightarrow \infty} \lambda_a(N) = \lambda_a$. The location of zeros of $G_N(a, t)$ in the t -plane can be scaled with $\lambda_a(N)$ in order to approximate the zeros of $g_N(a, t)$ (see equation (18)). The approximation will become increasingly accurate with increasing N .

In figure 2 the approximate zeros of $g_{10}(1, t)$ are plotted in the t -plane. This shows that, even for this small value of N , the estimated zeros are distributed close to the unit circle and spaced in a way consistent with approaching a uniform distribution in the limit as $N \rightarrow \infty$.

The location of the zeros in figure 2 can be examined by fitting a least squares ellipse to the data points. This has approximate centre at the point (0.011, 0), close to the origin, approximate half short axis of length 1.00 and approximate half long axis of length 1.01. The rays from the origin in figure 2 are the spokes of a regular 11-gon and they intersect the unit circle in the vertices of a regular 11-gon; each intersection is

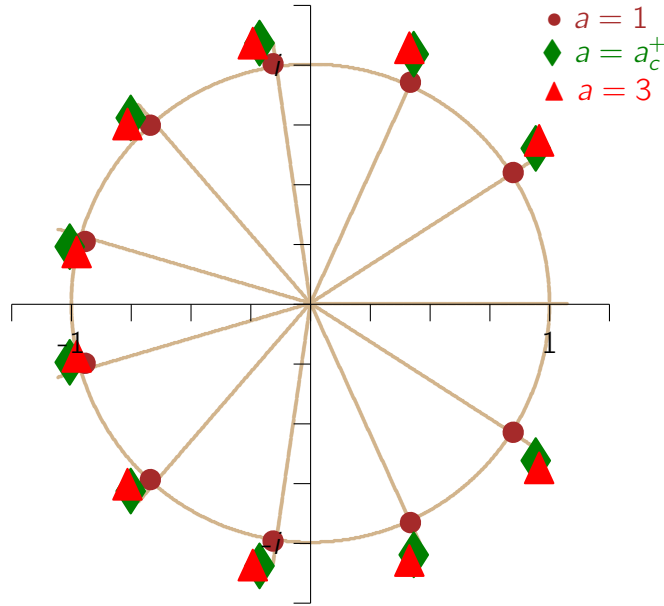


Figure 7: Approximate locations of the zeros of $g_N(a, t)$ for $N = 10$ and for $a = 1$ (\bullet), $a = 1.779 \approx a_c^+$ (\blacklozenge), and $a = 3$ (\blacktriangle). The zeros are close to the unit circle, and close to ten vertices of a regular 11-gon with centre at the origin, and one corner at the point $(1, 0)$, as illustrated. The rays from the origin are the spokes of a regular 11-gon.

close to a zero of $g_{10}(1, t)$, except at the point $(1, 0)$ on the real axis where there is no zero nearby.

The locations of zeros of $g_N(a, t)$ are, in general, functions of a (and of N). This is examined in figure 7 for $N = 10$ and three different values of a , namely $a = 1$ (the same data as in figure 2), $a = 1.779 \approx a_c^+$, and $a = 3$ (at this value the model is in the adsorbed phase). There are small movements in the zeros with increasing a , and this can be collectively examined by determining the least squares ellipse for each value of a . For $a = 1$ the least squares ellipse was given above (approximate centre at $(0.011, 0)$, approximate half short axis of length 1.00 and approximate half long axis of length 1.01). The ellipse for $a = 1.779$ has values $(0.049, 0)$, 1.125 and 1.139 for its approximate centre, half short axis, and half long axis. For $a = 3$ the values are $(0.077, 0)$, 1.137 and 1.168 for its approximate centre, half short axis, and half long axis.

The situation is similar for larger values of N . For example, the cases for $N = 100$ are illustrated in figures 8 and 9. In figure 8 the zeros of $g_N(a, t)$ with $N = 100$ and $a = 1$ are shown. These zeros are very close to 100 vertices of a regular 101-gon on the unit circle with one vertex at $(1, 0)$ (and this is the one vertex not close to a zero of $g_N(a, t)$). The least squares ellipse through the zeros has approximate centre $(0.0014, 0)$, approximate half short axis 1.001 and approximate half long axis 1.002.

In figure 9 the zeros are displayed for larger values of a . There are very little motions of the zeros with increasing a . For example, for $a = 1.779 \approx a_c^+$ the least squares ellipse through the zeros has approximate centre $(0.0068, 0)$, half short and half long axes of

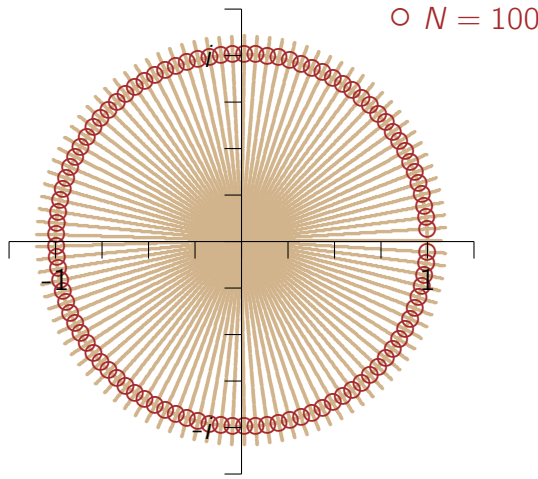


Figure 8: Approximate locations of the zeros of $g_N(a, t)$ for $N = 100$ and $a = 1$. The zeros are approximately on the unit circle, and close to 100 vertices of a regular 101-gon with centre at the origin, and with one corner at the point $(1, 0)$, as shown.

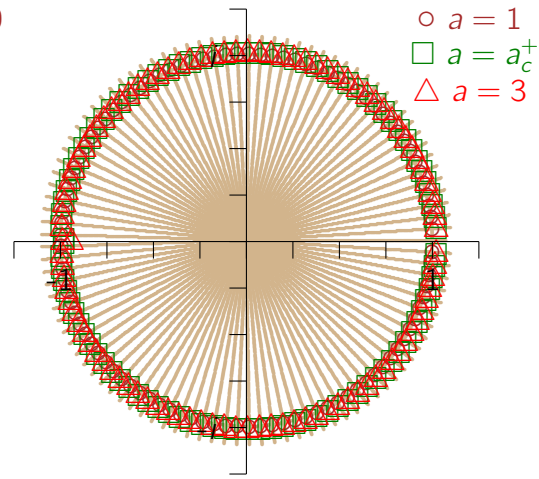


Figure 9: Approximate locations of the zeros of $g_N(a, t)$ for $N = 100$ and for $a = 1$, $a = 1.779 \approx a_c^+$, and $a = 3$. All these zeros are located very close to the unit circle.

approximate lengths 1.012 and 1.016. Similarly, for $a = 3$, the least squares ellipse has approximate centre at $(0.0101, 0)$, and half short and half long axes of approximate lengths 1.013 and 1.019.

In general, the zeros of $G_N(a, t)$ are accumulating on a circle of radius λ_a in the t plane, while the zeros of $g_N(a, t)$ are accumulating on the unit circle, also in the t -plane. The positions of the zeros are also close to N vertices of a regular $(N+1)$ -gon with vertices on the circle, and one vertex on the positive real axis which does not have a zero nearby. For even N the zeros are found in complex conjugate pairs, and for odd N there are $N-1$ zeros in complex conjugate pairs, and one additional zero located on the negative real axis. Increasing N (as a time variable) creates the illusion that new zeros are generated on the negative real axis, and the existing zeros in the upper half plane move clockwise along the circle (and in the lower half plane move anti-clockwise along the circle), while maintaining a distribution close to the vertices of a regular N -gon on the unit circle. This increases the density of zeros on the circle in a way which becomes uniform in the limit $N \rightarrow \infty$. By theorem 2.4 the zeros approach a uniform distribution on the circle in the limit as $N \rightarrow \infty$. This circle should become a natural boundary of the generating function $G(a, t)$ (see equation (12)) in the t -plane.

4.2. Fisher or partition function zeros

The partition function $A_n^+(a)$ (see equation (7)) was approximated using the approximate enumeration data obtained by the GAS algorithm for adsorbing walks in \mathbb{L}_+^2 [24]. The locations of zeros of $A_n^+(a)$ were obtained to high accuracy by using Maple [36]. In figure 10 the zeros are shown for small values n , namely $n \in \{25, 50, 75, 100\}$,

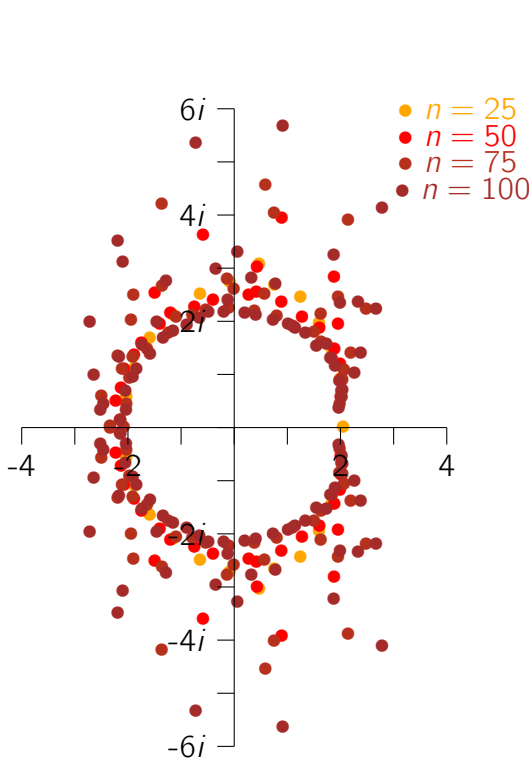


Figure 10: Approximate locations of the Fisher zeros of $A_n^+(a)$ for $n \in \{25, 50, 75, 100\}$. The zeros scatter in the a -plane, outlining a disk centred at the origin which is free from zeros. There are no zeros on the positive real axis, but an edge singularity is clearly being formed at a_c^+ . A positive fraction of the zeros appear to accumulate on a circle of radius a_c^+ .

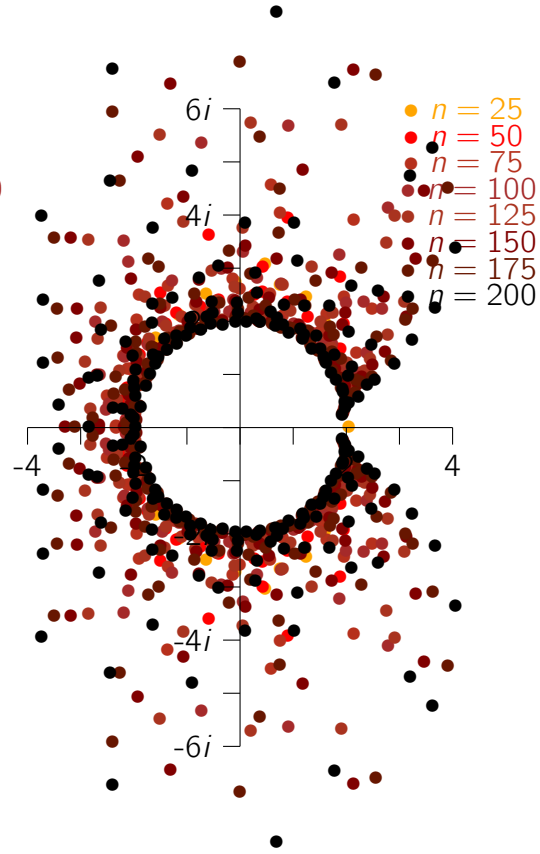


Figure 11: Approximate locations of the Fisher zeros of $A_n^+(a)$ for $n \in \{25, 50, \dots, 175, 200\}$. These data include all the data in figure 10. Notice that the zeros appear to pinch the positive real axis to create an edge singularity at the critical point a_c^+ . A positive fraction of the zeros appear to accumulate on a circle of radius a_c^+ .

and in figure 11 for values of n in steps of 25 to $n = 200$. These data suggest that the zeros form a characteristic pattern in the a -plane, such that a fraction is accumulating on a circle (called the *critical circle*), while the remaining zeros distribute in the a -plane outside the critical circle. The results for larger values of n , namely $n \in \{100, 200, 300, 400, 500\}$, are plotted in figure 12.

By theorem 2.8 there exists a $\rho \in (0, 1)$ such that a positive fraction of zeros will be in an annulus centred at the origin and of inner radius $r = |a| = 1 - \rho$ and outer radius $r = |a| = \frac{1}{1 - \rho}$.

The zeros plotted in figure 12 appear to accumulate on a circle in the a -plane with increasing n . However, many zeros are also found away from this circle, and they do in fact appear to drift away from the origin with increasing n . These observations are not inconsistent with theorem 2.8. In fact, it appears that many zeros are restricted

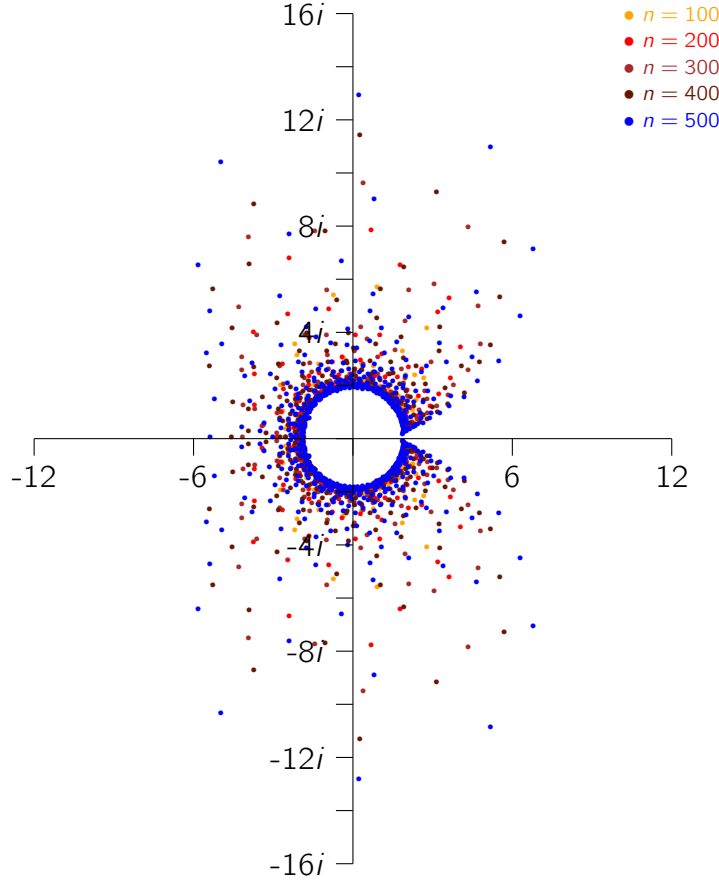


Figure 12: Partition functions zeros of the partition function $A_n^+(a)$ of two dimensional adsorbing walks in the a -plane. The zeros appear to be distributed outside a circle of radius a_c^+ (the critical circle) and inside a vertical strip of width w which seems to increase with n .

to an annulus containing the circle and their angular distribution seems quite uniform (consistent with theorem 2.9), except in the vicinity of the positive real axis, where some zeros are converging (with increasing n) to the critical adsorption point a_c^+ .

The finite size *excess free energy* $F_N^e(a)$ can be computed using equation (22):

$$F_n^e(a) = F_n(a) - \log c_n^{(d-1)} = \sum_{k=1}^n \log(a - a_k). \quad (77)$$

The finite size *energy* $E_n(a)$ per unit length and *specific heat* $C_n(a)$ are the first and second derivatives of $F_n^e(a)$ to $\log a$, divided by length n :

$$E_n(a) = \frac{a}{n} \frac{d}{da} F_n^e(a) = \frac{a}{n} \sum_{k=1}^n \frac{1}{a - a_k}, \quad \text{and} \quad C_n(a) = a \frac{d}{da} E_n(a) = -\frac{a}{n} \sum_{k=1}^n \frac{a_k}{(a - a_k)^2}. \quad (78)$$

The specific heat $C_n(a)$ has limiting behaviour $\lim_{n \rightarrow \infty} C_n(a) \sim (a - a_c^+)^{-\alpha}$, where $2 - \alpha = \frac{1}{\phi}$, and α is the specific heat exponent, while ϕ is the crossover exponent of adsorbing walks. It is thought that $\phi = \frac{1}{2}$ in all dimensions (numerical results in reference [25] gives $\phi = 0.5005 \pm 0.0036$), so α is close to or equal to 0. That is, $C_n(a_c^+) \rightarrow \text{constant}$ as $n \rightarrow \infty$, and since $\mathcal{A}^+(a)$ is a constant when $a < a_c^+$ (see

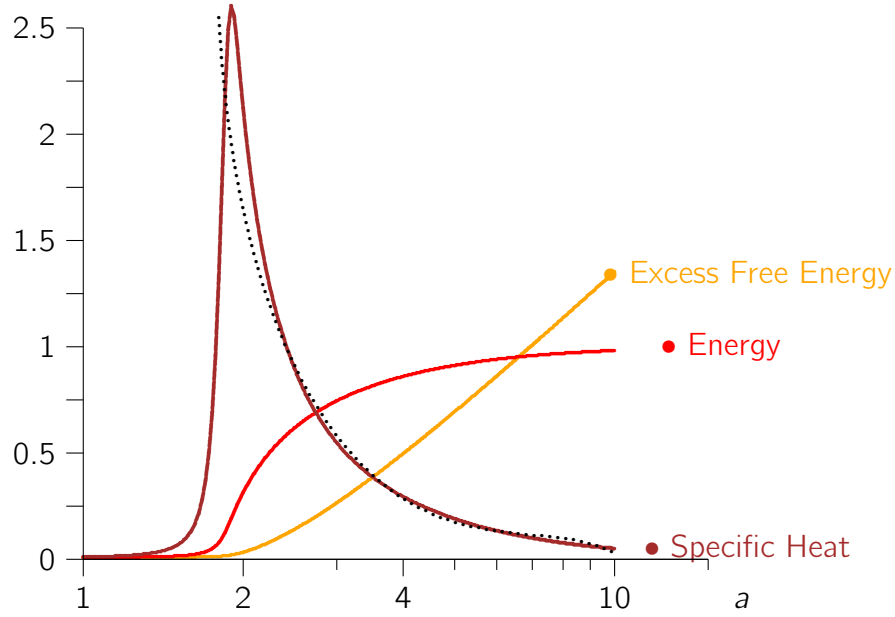


Figure 13: The excess free energy $F_n^e(a)$ in the a -plane for two dimensional adsorbing walks of length $n = 500$ (see equation (77)), plotted as a function of a on a semilogarithmic graph. The function is convex in $\log a$. The energy per unit length, and the specific heat, are plotted on the same graph, and were computed as shown in equation (78). The specific heat shows a sharp peak and is approximated by the dotted curve (see equation (80)).

equation (9)), one may consider

$$\lim_{n \rightarrow \infty} C_n(a) \begin{cases} = 0, & \text{if } a < a_c^+; \\ \simeq A_0 - B_0(a - a_c^+)^\phi, & \text{if } a > a_c^+, \end{cases} \quad (79)$$

provided that the activity a is not much larger than a_c^+ . A least squares fit with $\phi = \frac{1}{2}$ and the model

$$C_n(a) = A_0 - B_0\sqrt{a - a_c^+} - C_0(a - a_c^+) - D_0(a - a_c^+)^{1.5} \quad (80)$$

to data for $n = 500$ gives the dotted curve in figure 13 (where $A_0 = 3.096$, $B_0 = -3.785$, $C_0 = 1.626$ and $D_0 = -0.237$), approximating the shape of the specific heat curve well as a increases from a_c^+ .

Equation (44) shows that $E_n(a)$ approaches zero as $n \rightarrow \infty$ and $a < a_c^+$. Consequently, $C_n(a) \rightarrow 0$ as $n \rightarrow \infty$ and $a < a_c^+$. Similarly, equation (44) shows that $E_n(a)$ approaches a constant as $n \rightarrow \infty$ and $a \rightarrow \infty$. That is, $C_n(a) \rightarrow C(a) \geq 0$ if $a > a_c^+$ and $n \rightarrow \infty$ (where $C(a)$ is the limiting specific heat). It is therefore reasonable to expect that $C_n(a_c^+) = C_m(a_c^+)$ at the adsorption critical point a_c^+ for two different values of n and m . Solving for a_c^+ from the equation $C_n(a) = C_m(a)$ for $m = 2n$, and $n \in \{200, 210, 220, 230, 240, 250\}$, gives estimates which are stable to three significant digits. Taking the average gives the estimate

$$a_c^+ = 1.765, \quad \text{in the square lattice,} \quad (81)$$

where the last digit is uncertain. This compares well with the result from series enumeration $a_c^+ = 1.77564$ [2]. The curves in figure 13 are determined from the

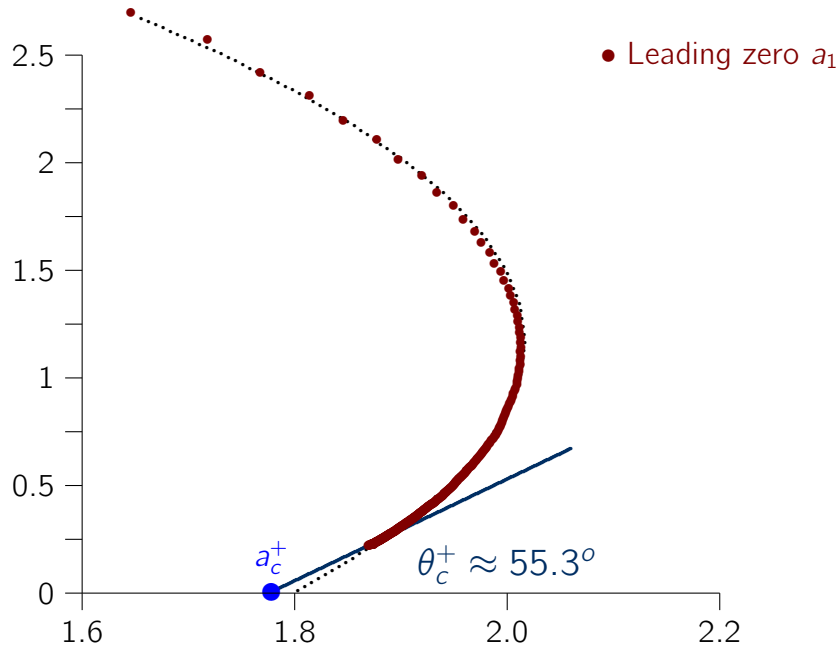


Figure 14: The trajectory of the leading Fisher zero a_1 as a function of n for adsorbing walks in the square lattice. With increasing n the leading zero approaches the real axis, where it, and its complex conjugate, squeeze an edge singularity in the limiting free energy of the model at the critical adsorption point a_c^+ . The dotted line is a least squares parabolic curve fitted to the trajectory of the leading zero. Assuming a critical point at $a_c^+ = 1.77564$ [2] allows one to estimate the angle of incidence $\theta_c^+ \approx 55.3^\circ$. The approximating parabola intersects the real axis at the estimated critical point 1.8049 at a critical angle of size 58.2° . If the least squares parabola is constrained to pass through the estimated critical point at 1.77564, then the critical angle has approximate size 53.7° .

estimated locations of partition function zeros, from which the estimate for a_c^+ above is determined. This compares well with the result in reference [24], namely $a_c^+ = 1.779 \pm 0.003$, which was determined using approximate enumeration data generated with the GAS algorithm and analysed using conventional statistical methods.

The *leading Fisher zero*, denoted by a_1 , is that zero of $A_n^+(a)$ with smallest principal argument in the first quadrant in the a -plane. The leading zero a_1 is a function of n , and it, and its conjugate \bar{a}_1 , converge to the edge singularity at a_c^+ on the positive real axis as $n \rightarrow \infty$. Thus, as n increases, then $\Im a_1 \rightarrow 0$ and $\Re a_1 \rightarrow a_c^+$. The rate at which a_1 moves to the real axis should be controlled by the crossover exponent ϕ of adsorbing walks. Since it is thought to be the case that $\phi = \frac{1}{2}$ in all dimensions $d \geq 2$ [3], one may expect that $\Im a_1 \sim \frac{c}{\sqrt{n}}$ and $\Re a_1 \sim a_c^+ + \frac{c}{\sqrt{n}}$.

The trajectory of a_1 in the first quadrant as n increases is shown in figure 14 for adsorbing walks in \mathbb{L}_+^2 , and for $n \in [10, 500]$. The estimate $a_c^+ = 1.77564$ is denoted by a bullet on the real axis (see reference [24]). With increasing n the trajectory of a_1 tends to straighten out and it approaches the real axis at a critical angle θ_c^+ of about 55.3° .

The leading zeros appear to accumulate on a curve which may be approximated by a quadratic curve in the a -plane. If it is assumed that $\Re a_1 = a_c^+ + \alpha_0 \Im a_1 + \alpha_1 (\Im a_1)^2$,

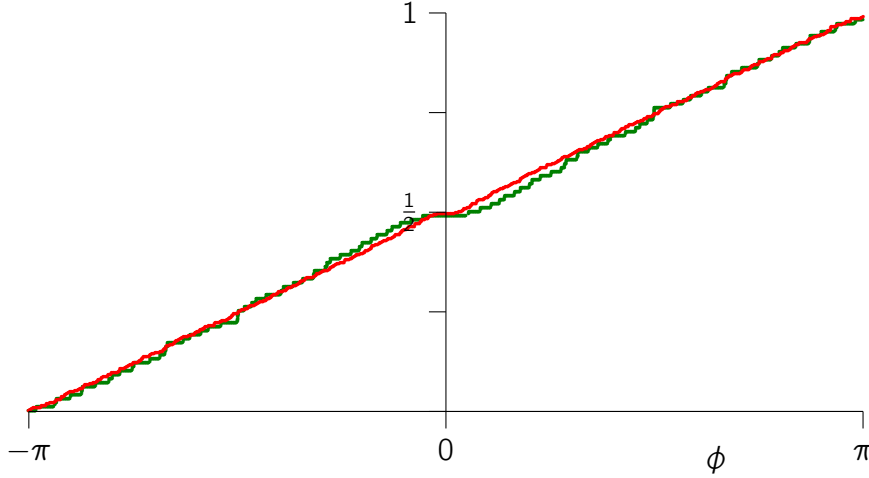


Figure 15: The cumulative angular distribution function $\frac{1}{n}\alpha_n(-\pi, \phi)$ of Fisher zeros (displayed for $n = 400$ and $n = 500$; see equation (84)), plotted as a function of ϕ , for adsorbing walks in the square lattice. The curves are smoother for larger values of n , and by equation (56), approach a limiting curve bounded by $\lim_{n \rightarrow \infty} \frac{1}{n}\alpha_n(-\pi, \phi) \leq \min\{1, \frac{1}{\pi}\phi + 1\}$. The data suggest that $\lim_{n \rightarrow \infty} \frac{1}{n}\alpha_n(-\pi, \phi) = \frac{1}{2\pi}\phi + \frac{1}{2}$.

then a least squares fit to the data in figure 14 gives

$$\Re a_1 = 1.8049 + 0.6003 \Im a_1 - 0.4298(\Im a_1)^2. \quad (82)$$

This gives the estimate $a_c^+ \approx 1.8009$ and angle of incidence $\theta_c^+ = 90^\circ - \arctan 0.6190 \approx 58.2^\circ$ (slightly larger than the 55.3° calculated above). It seems that the trajectory is fitted well by a quadratic curve, but the values of the critical point a_c^+ and the critical angle θ_c^+ obtained in this way are slightly larger than the estimates obtained earlier, but not numerically inconsistent with those values.

Repeating the analysis above, but now with the critical value fixed at $a_c^+ = 1.77564$, gives the least squares parabola

$$\Re a_1 = 1.77564 + 0.7347 \Im a_1 - 0.5220(\Im a_1)^2. \quad (83)$$

This gives the angle of incidence $\theta = 90^\circ - \arctan 0.7349 \approx 53.7^\circ$ (an angle slightly smaller than calculated above).

The *cumulative angular distribution function* $\alpha_n(\phi)$ of the Fisher zeros of $A_n^+(a)$ around the origin in the a -plane is given by

$$\alpha_n(\phi) = \frac{1}{n} \alpha_n(-\pi, \phi) \quad (84)$$

for adsorbing walks of length n (and where $\alpha_n(\theta, \phi)$ is defined in equation (15)). This is the fraction of Fisher zeros with (complex) principal argument in the interval $(-\pi, \phi]$, and it increments by $\frac{1}{n}$ each time a new zero enters the interval $(-\pi, \phi]$ with increasing ϕ .

The cumulative angular distribution function is plotted in figure 15 for adsorbing walks in \mathbb{L}_+^2 for $n = 400$ and $n = 500$. The function increases steadily, except near $\phi = 0$ where it has a constant part which steadily decreases in length as n increases (this corresponds to the gap between leading Fisher zeros and the positive real axis near $\phi = 0$).

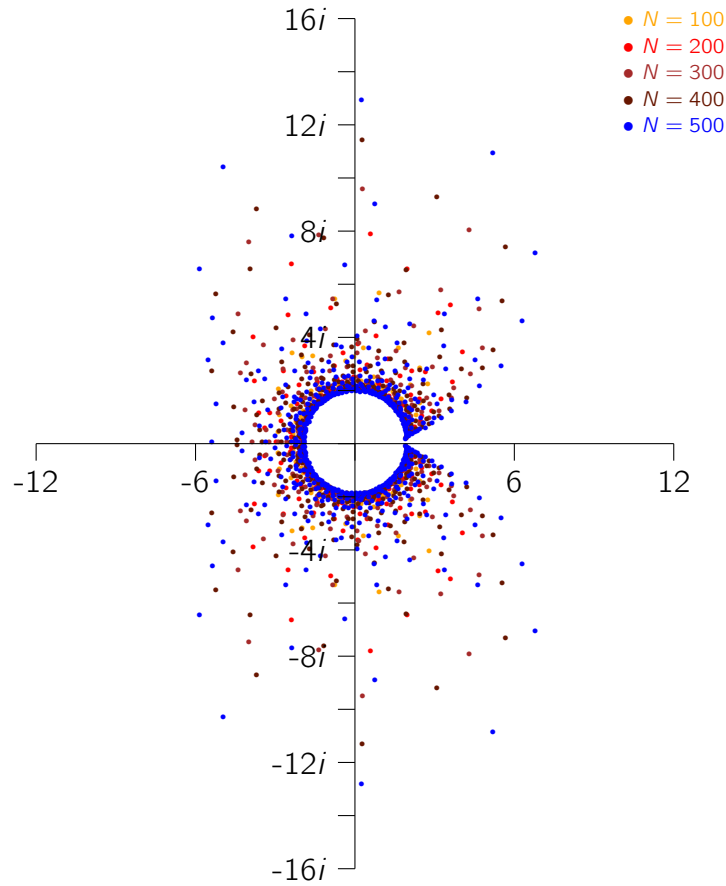


Figure 16: Zeros of $G_N(a, t)$ (Yang-Lee zeros) in the a -plane for $t = \frac{1}{\mu_2}$. The general distribution of the zeros is similar to that seen for Fisher zeros (see figure 12). There are also little dependence on the value of t . With increasing N the leading zero and its conjugate approaches the positive real axis at a_c^+ , creating an edge singularity in the limit as $N \rightarrow \infty$.

4.3. Yang-Lee zeros (a -plane zeros of $G_N(a, t)$)

The zeros of the partial generating function $G_N(a, t)$ (equation (14)) in the a -plane are closely related to Fisher (partition function) zeros. To distinguish these zeros from Lee-Yang zeros (which are t -plane zeros of $G_N(a, t)$), they will be called *Yang-Lee zeros*.

The analysis of Yang-Lee zeros proceeds similar to Fisher zeros (as in section (4.2)). The zeros were determined by deflating $G_N(a, t)$ for $t = \frac{1}{\mu_2}$ and are plotted in figure 16 for $N \in \{100, 200, 300, 400, 500\}$. In general, the location of zeros did not change in significant ways with changes in the value of t . The results for these zeros are very similar to those results seen for Fisher zeros. For example, the trajectory of the leading zero is very similar to figure 14, and the cumulative angular distribution of zeros has the same profile as seen in figure 15.

4.4. The density profile and distribution of Fisher and Yang-Lee zeros

Partition function zeros in figure 12, or Yang-Lee zeros in figure 16, have angular and radial distribution profiles around the origin in the a -plane. The angular distribution of

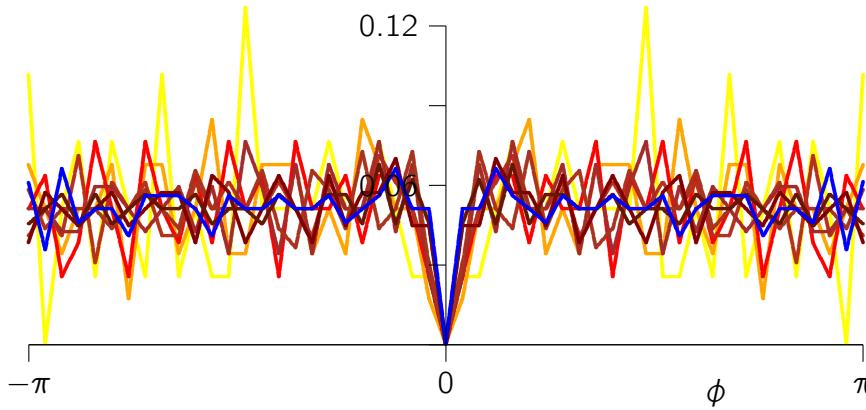


Figure 17: The angular distribution of partition function zeros in the square lattice estimated by plotting $\frac{50}{2\pi n} \alpha_n(\frac{(2m-1)\pi}{100}, \frac{(2m+1)\pi}{100})$ against $\frac{2m\pi}{50}$ for $m = -25, -24, -23, \dots, 24, 25$, and for $n \in \{100, 200, \dots, 500\}$. The darker colours correspond to larger values of n , and the data points are interpolated by line segments. The data become less noisy with increasing n and there is a notable decrease (to zero) of the density of zeros close to the real axis (where $\phi = 0$).

Fisher zeros was already examined in figure 15, and the same approach to Yang-Lee zeros gives a result which is similar to this.

The distribution function $\alpha_n(\theta, \phi)$ is given by

$$\alpha_n(\theta, \phi) = n \alpha_n(\phi) - n \alpha_n(\theta), \quad (85)$$

and this may be estimated from the data in figure 15. This gives a nearly uniform distribution, except for a small gap where the distribution decreases for angles near 0. This is consistent with the suggestion of theorem 2.11 on the angular distribution of Fisher zeros.

An alternative approach to the angular distribution function is to count zeros in wedges with vertices at the origin (and where the vertices of the wedges have size $\frac{2\pi}{M}$ in the a -plane). If $M = 50$ then the a -plane is partitioned into 50 wedges and the zeros are binned and counted in each wedge. This gives results as shown in figure 17 for $n \in \{100, 200, \dots, 500\}$. The darker colours correspond to larger values of n , and the figure is obtained by plotting $\frac{50}{2\pi n} \alpha_n(\frac{(2m-1)\pi}{100}, \frac{(2m+1)\pi}{100})$ against $\frac{2m\pi}{50}$ for $m = -25, -24, \dots, 25$, with the points interpolated by line segments. The graph is very uneven for small n , but this unevenness decreases as n increases. Also notable is the low density in a (narrow) wedge containing the positive real axis.

Plotting Yang-Lee zeros instead of Fisher zeros gives very similar looking results.

In the radial direction Fisher zeros appear to accumulate on the critical circle $|a| = a_c^+$ in the a -plane. The fraction of zeros inside or outside a disk $|a| < r$ is a function of n , and may be approaching limiting values as n increases to infinity. This is tested in figure 18. The data points marked by $|a| < 2.0$ correspond to the fraction of zeros inside the disk $|a| \leq 2$ (this is the same as the fraction of zeros inside the annulus $a_c^+ \leq |a| \leq 2$). The fraction is small for $n < 100$, but increases steadily and appears to approach a constant fraction of about 0.30 for $n > 300$.

A similar situation is seen for zeros farther away from the origin. For example, the fraction of zeros farther away than a distance of 2.0 from the origin (that is, the fraction

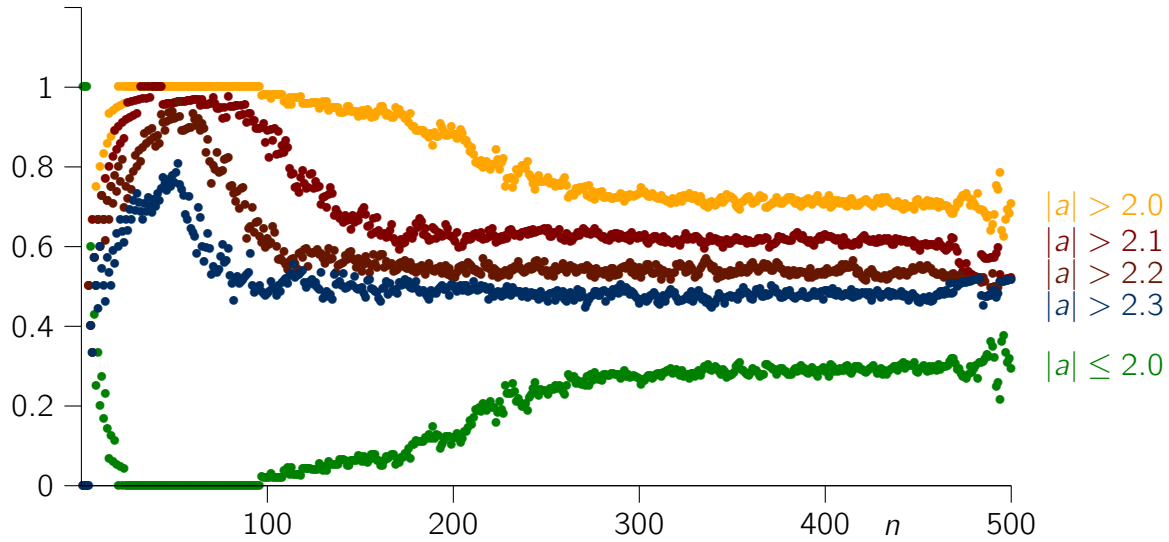


Figure 18: The fraction of partition function zeros (zeros of $A_n^+(a)$ in the a -plane) of adsorbing walks in the square lattice. The data displayed show the fraction of zeros at distances closer than 2 (green points along the lowest curve), and then farther away than 2, 2.1, 2.2 and 2.3 from the origin in the a -plane. Determining the same data for Yang-Lee zeros (zeros of $G_N(a, t)$ with $t = \frac{1}{\mu_2}$) gives a similar result, with data points which largely coincide with the data plotted here. The data appear to flatten to constant values with increasing n . This suggests that the number density of zeros decreases inversely with distance from the origin if $|a|$ is large and in the limit that $n \rightarrow \infty$.

of zeros outside a disk $|a| \leq 2$ at the origin), is shown by the data points accumulating along the top curve of the graph in figure 18. For small values of n the fraction is nearly equal to 1, but this decreases and levels off at about 0.70 for $n > 300$.

The data outside a disk $|a| \leq r$ decreases with increasing r , as seen for $r \in \{2.0, 2.1, 2.2, 2.3\}$ in figure 18. In each case the fraction of zeros levels off (within noise) to a constant, independent of n . The results for Yang-Lee zeros (zeros of $G_N(a, t)$) with $t = \frac{1}{\mu_2}$ are similar to the results for Fisher zeros shown in figure 18.

The results in figure 18 suggest that only a fraction of Fisher and Yang-Lee zeros accumulate on the critical circle $|a| = a_c^+$. That is, it appears that a constant fraction of zeros accumulate on the critical circle, while the inside of the critical circle is empty, and the remaining zeros are distributed outside the critical circle in the a -plane. The radial density (integrated in the angular direction) approaches a constant value with increasing n . This suggests, in the limit as $n \rightarrow \infty$, that there are zeros at arbitrary distances from the origin. However, since the distribution of zeros is integrable, the *number density* of zeros should drop off faster than the inverse squared distance from the origin.

5. Numeral Results in the Cubic Lattice

5.1. Lee-Yang zeros of $G_N(a, t)$ in the cubic lattice

Similar to the results in the square lattice, the Lee-Yang zeros of $G_N(a, t)$ will accumulate on a circle of radius λ_a (see equation (16)) as $N \rightarrow \infty$ in the t -plane. By scaling t with

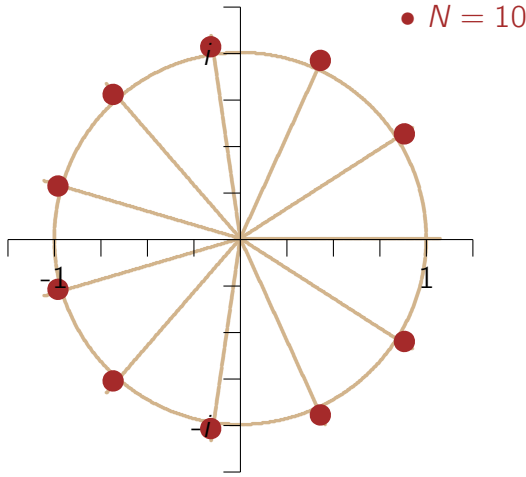


Figure 19: Approximate locations of the zeros of $g_N(a, t)$ for $N = 10$ and $a = 1$ in the cubic lattice. The zeros are located approximately on the unit circle, and close to 10 vertices of a regular 11-gon with centre at the origin (oriented with one vertex at the point $(1,0)$). The rays from the origin are the spokes of the regular 11-gon.

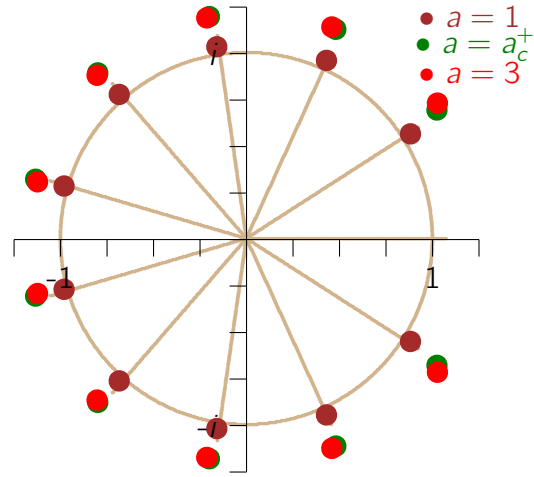


Figure 20: Approximate locations of the zeros of $g_N(a, t)$ for $N = 10$ and for $a = 1$, $a = 1.306 \approx a_c^+$, and $a = 3$ in the cubic lattice. The zeros for $a > 1$ have moved slightly away from the unit circle, but are still fairly close to it.

λ_a (see equation (18)), the Lee-Yang zeros will accumulate on the unit circle in the t -plane (by theorem 2.2), and their distribution will be (asymptotically) uniform in the limit as $N \rightarrow \infty$.

The Lee-Yang zeros will be examined by considering the partial sum $g_N(a, t)$ in equation (18) for data obtained for \mathbb{L}_+^3 . The estimated locations of these zeros are shown in figures 19 and 20, for $N = 10$ and $a = 1$, and for $a \in \{1, a_c^+, 3\}$, respectively, where a_c^+ is the critical adsorption activity estimated in reference [24] ($a_c^+ \approx 1.306$).

The best least-squares ellipse through the zeros in figure 19 has centre at $(0.012, 0)$, half short axis of length 1.031 and half long axis of length 1.042. The rays from the origin in this figure intersect the unit circle in the vertices of a regular 11-gon (with one vertex on the real axis). Each vertex of the 11-gon is close to a Lee-Yang zero, except for the vertex on the real axis.

In figure 20 the dependence of the Lee-Yang zeros on the value of a is examined. The data plotted in this figure correspond to $a \in \{1, a_c^+, 3\}$ with a_c^+ approximated by 1.306 [24]. For both $a = 1.306$, and $a = 3$, the zeros have moved slightly off the unit circle, but they are still located on a least squares ellipsoid with centre close to the origin (in the case of $a = 1.306$, with centre at $(0.0286, 0)$, half short axis of approximate length 1.207 and half long axis of approximate length 1.211; and for $a = 3$, with centre at $(0.0487, 0)$, half short axis of approximate length 1.209 and half long axis of approximate length 1.216).

The data for $N = 100$ are shown in figures 21 and 22. The zeros are evenly

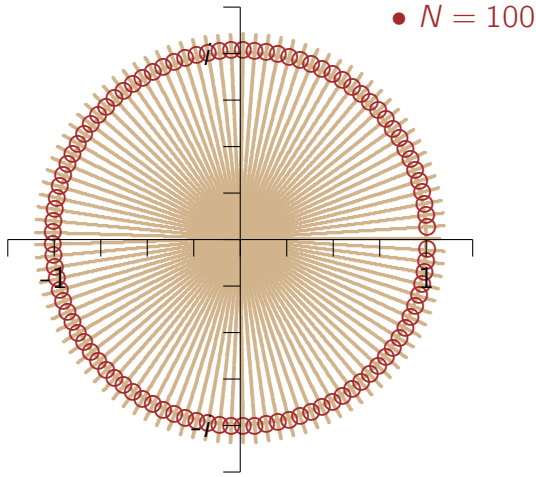


Figure 21: Approximate locations of the zeros of $g_N(a, t)$ for $N = 100$ and $a = 1$ in the cubic lattice. The zeros are approximately on the unit circle, and close to 100 vertices of a regular 101-gon with centre at the origin, and oriented with one vertex at the point $(1, 0)$.

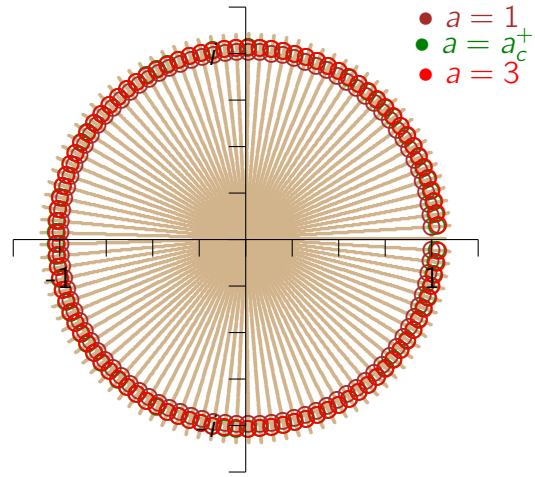


Figure 22: Approximate locations of the zeros of $g_N(a, t)$ for $N = 100$ and for $a = 1$, $a = 1.306 \approx a_c^+$, and $a = 3$ in the cubic lattice. All the zeros are close to the unit circle. As in figure 21 the rays are the spokes of a regular 101-gon.

distributed along the unit circle for $a = 1$ in figure 21, close to the vertices of a regular 101-gon with centre at the origin and one vertex on the positive real axis at the point $(1, 0)$. The best least-squares ellipse through these zeros has centre at $(0.001, 0)$, approximate half short axis of length 1.001 and approximate half long axis of length 1.011. Changes in the values of a do not have a significant effect on the location of the zeros of $g_N(a, t)$, since these are already scaled by estimates of λ_a . Thus, the zeros for $a \in \{1, a_c^+, 3\}$ shown in figure 22 are all close to the unit circle and are evenly distributed along it. The best least-squares ellipse through the zeros when $a = 1.306$ in figure 22 has centre $(0.003, 0)$, half short axis of approximate length 1.026 and half long axis of approximate length 1.026. If $a = 3$, then the least squares ellipse has centre at $(0.006, 0)$, half short axis of approximate length 1.025 and half long axis of approximate length 1.027.

5.2. Fisher or partition function zeros

The partition function $A_n^+(a)$ of adsorbing walks in \mathbb{L}_+^3 was approximated using the approximate microcanonical data obtained from the GAS algorithm simulation for adsorbing walks in reference [24]. The locations of zeros in the complex plane were similarly determined by deflating the polynomials using Maple [36]. The results for $n \in \{25, 50, 75, 100\}$ are plotted in figure 23, and for $n \in \{100, 200, \dots, 500\}$ are shown in figure 24.

By theorem 2.8 a positive fraction of partition function zeros will be located in an annulus $\{a \mid 1 - \rho \leq r \leq \frac{1}{1 - \rho}\}$ for some value of $\rho \in (0, 1)$.

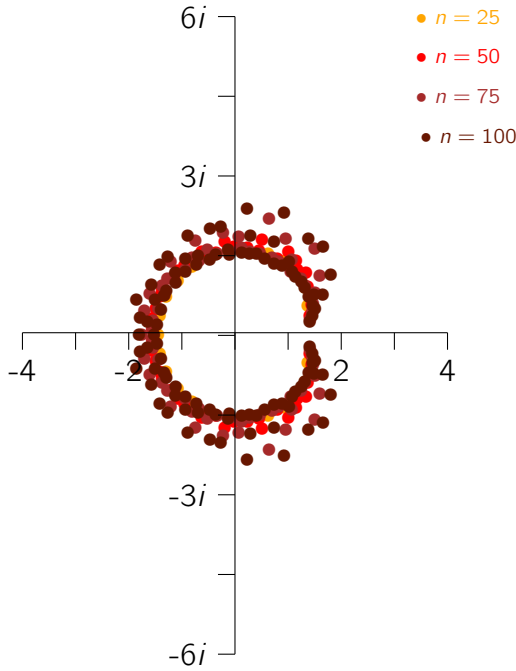


Figure 23: Partition function (Fisher) zeros of $A_n^+(a)$ in the a -plane for adsorbing walks in the cubic lattice, for $n \in \{25, 50, 75, 100\}$.

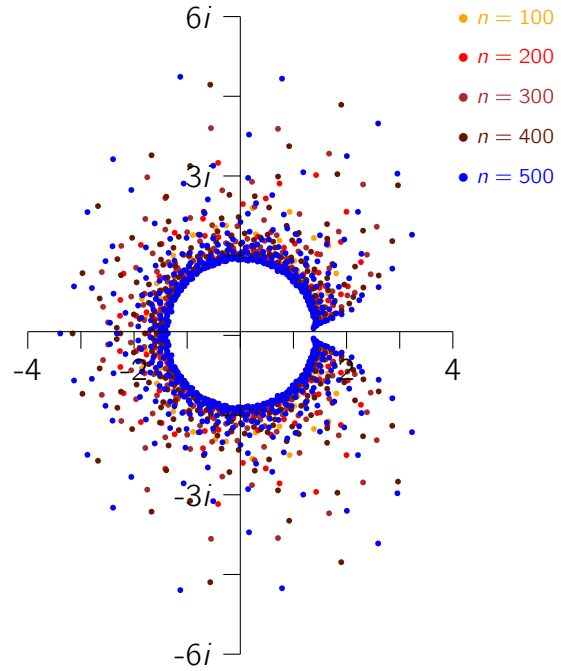


Figure 24: Partition function (Fisher) zeros of $A_n^+(a)$ in the a -plane for adsorbing walks in the cubic lattice, for $n \in \{100, 200, 300, 400, 500\}$.

The zeros plotted in figure 24 appear to accumulate on a circle in the a -plane with increasing n . However, many zeros are also distributed away from this circle, and with increasing n zeros are found at further distances from the origin. These observations are not inconsistent with theorem 2.8. Many zeros are located in an annulus containing the circle of critical radius a_c^+ (by theorem 2.12) and their angular distribution appears to be very even, except in the vicinity of the positive real axis, where the leading zeros are converging to the edge singularity (with increasing n) at the critical adsorption point a_c^+ .

The finite size *excess free energy* $F_n^e(a)$ can be computed using equation (22):

$$F_n^e(a) = F_n(a) - \log c_n^{(d-1)} = \sum_{k=1}^n \log(a - a_k). \quad (86)$$

The finite size *energy* $E_n(a)$ per unit length and *specific heat* $\mathcal{C}_n(a)$ are the first and second derivatives of $F_n^e(a)$ to $\log a$, divided by length n (see equation (78)). Assuming that the specific heat $\mathcal{C}_n(a)$ has limiting behaviour as shown in equation (79) with $\phi = \frac{1}{2}$, then $\mathcal{C}_n(a)$ should be given by equation (78) when $a > a_c^+$ in the limit as $n \rightarrow \infty$. A least squares fit gives the dotted curve in figure 25 (where $A_0 = 4.123$, $B_0 = -5.987$, $C_0 = 2.852$ and $D_0 = -0.443$), approximating the shape of the specific heat curve well as a increases from a_c^+ .

Equation (79) shows that $\mathcal{C}_n(a) \rightarrow 0$ as $n \rightarrow \infty$ and $a < a_c^+$, and $\mathcal{C}_n(a) \rightarrow \mathcal{C}(a) \geq 0$ if $a > a_c^+$ and $n \rightarrow \infty$. It may reasonably be expected that $\mathcal{C}_n(a_c^+) = \mathcal{C}_m(a_c^+)$ at the critical point. Solving this for $m = 2n$ and for $n \in \{200, 210, 220, 230, 240, 250\}$, give estimates which are stable to three decimal places. Taking the average gives the estimate

$$a_c^+ = 1.326, \quad \text{in the cubic lattice,} \quad (87)$$

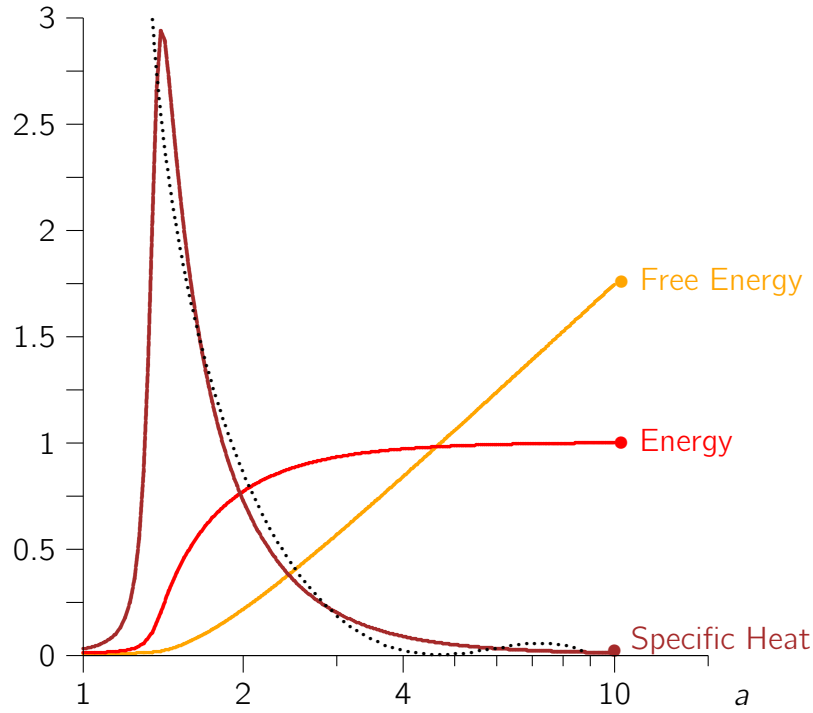


Figure 25: The excess free energy $F_n^e(a)$ in the a -plane for three dimensional adsorbing walks of length $n = 500$ (see equation (77)), plotted as a function of a on a semilogarithmic graph. The function is convex in $\log a$. The energy per unit length, and the specific heat, are plotted on the same graph, and were computed as shown in equation (78). The specific heat shows a sharp peak and is approximated by the dotted curve (see equation (80)).

where the last digit is uncertain. This compares well with (but is slightly larger than) the result obtained in reference [24], namely $a_c^+ = 1.306(7)$ [24].

The leading Fisher zeros a_1 are plotted in figure 26. The estimate $a_c^+ = 1.306$ from reference [24] is denoted by the bullet on the real axis. With increasing n zeros appear to move along a curve and it approaches the real axis at an angle θ as $n \rightarrow \infty$. A least squares fit to the curve, using the model $\Re a_1 = a_c^+ + \alpha_0 \Im a_1 + \alpha_1 (\Im a_1)^2$ gives

$$\Re a_1 = 1.340 + 0.4868 \Im a_1 - 0.8035 (\Im a_1)^2. \quad (88)$$

This gives the estimate $a_c^+ \approx 1.340$ and angle of incidence $\theta = 90^\circ - \arctan 0.4846 \approx 64.0^\circ$. The location of the leading zeros are well approximated by the quadratic curve, and this may indicate that the estimate in [24] slightly underestimates the location of the critical point.

Repeating the analysis above, but now with the critical value fixed at $a_c^+ = 1.306$ (so that the least squares parabola passes through the point a_c^+ on the real axis), gives

$$\Re a_1 = 1.306 + 0.7350 \Im a_1 - 1.10578 (\Im a_1)^2. \quad (89)$$

This gives the angle of incidence $\theta = 90^\circ - \arctan 0.7350 \approx 54.8^\circ$ (a smaller angle than calculated above).

The estimates for the critical angle above (namely 64.0° , and 54.8°) show that there remains significant uncertainty in its value.

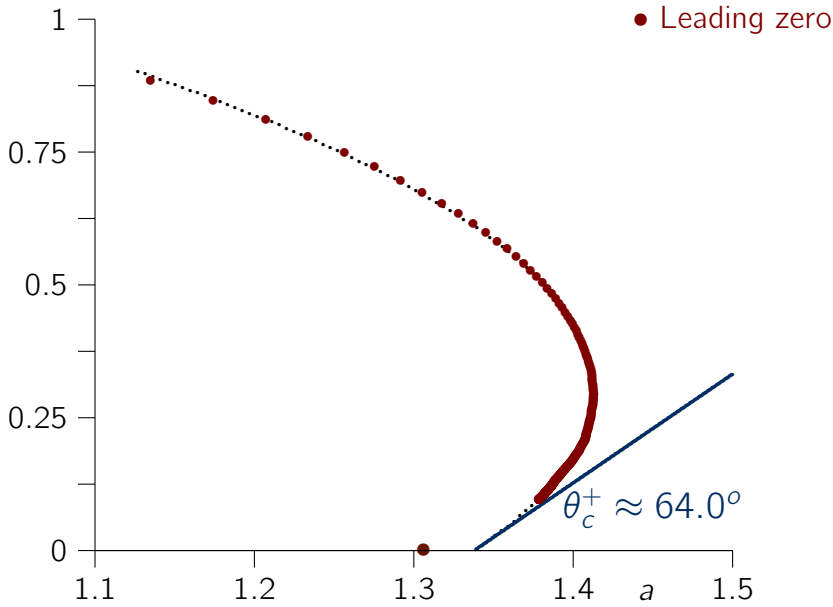


Figure 26: The trajectory of the leading Fisher zero a_1 as a function of n for adsorbing walks in the cubic. With increasing n the leading zero approaches the real axis, where it (together with its complex conjugate) squeeze an edge singularity in the limiting free energy of the model at the critical adsorption point a_c^+ (denoted by \bullet on the real axis). The dotted line is a least squares quadratic curve fitted to the trajectory of the leading zero. It intersects the real axis at the critical point, estimated in this way to be approximately equal to 1.34. The angle at which the curve intersects the real axis is about 64° . If the least squares parabola is constrained to pass through the estimated critical point $a_c^+ = 1.306$, then its angle of intersection is approximately 54.6° .

The *cumulative angular distribution function* $\mathbf{\alpha}_n(\phi)$ of the partition function zeros of adsorbing walks of length n around the origin in the a -plane is defined in equation (84) (where $\alpha_n(\theta, \phi)$ is defined in equation (15)). That it, $\mathbf{\alpha}_n(\phi)$ is the fraction of Fisher zeros with (complex) principal argument in the interval $(-\pi, \phi]$, and it increments in steps of size $\frac{1}{n}$ each time a new zero enters the interval $(-\pi, \phi]$ with increasing ϕ . $\mathbf{\alpha}_n(\phi)$ is plotted in figure 27 for adsorbing walks in \mathbb{L}_+^3 and for $n = 400$ and $n = 500$. For these finite values of n it is a step-function, with a wider constant part straddling the positive real axis where $\phi = 0$. The constant part steadily decreases in length as n increases (this corresponds to the leading Fisher zero approaching the real axis with increasing n).

The distribution function $\alpha_N(\theta, \phi)$ is given by

$$\alpha_n(\theta, \phi) = n \mathbf{\alpha}_n(\phi) - n \mathbf{\alpha}_n(\theta), \quad (90)$$

and this can be estimated from the data in figure (27). Polynomial fits to $\mathbf{\alpha}_n(\theta)$ give a very uniform profile for $\alpha_n(\theta, \phi)$, consistent with theorem 2.11 on the angular distribution of Fisher zeros.

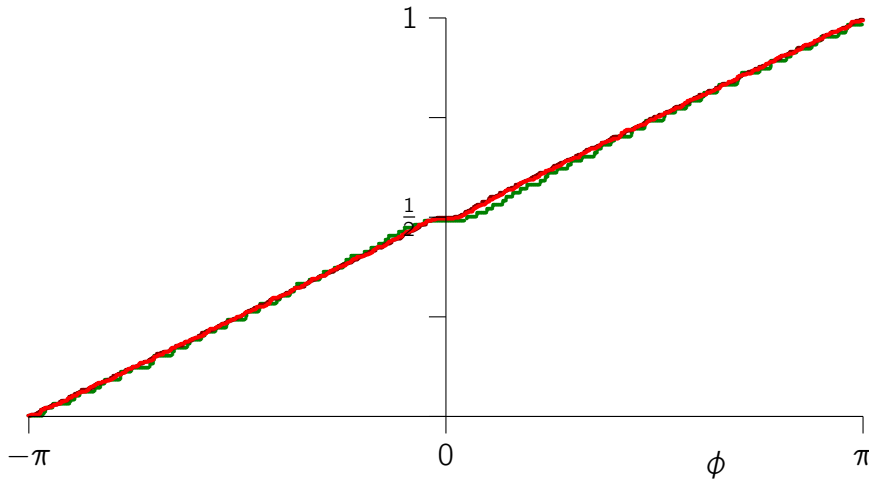


Figure 27: The cumulative angular distribution function of Fisher zeros of adsorbing walks in the cubic lattice, $\frac{1}{n} \alpha_n(-\pi, \phi)$ (displayed for $n = 400$ and $n = 500$ in the cubic lattice as a function of θ ; see equation (84)). These curves are step functions and they become smoother for larger values of n . By equation (56) the limit curve is bounded by $\lim_{n \rightarrow \infty} \frac{1}{n} \alpha_n(-\pi, \phi) \leq \min\{1, \frac{1}{\pi} \phi + 1\}$. The data suggest that $\lim_{n \rightarrow \infty} \frac{1}{n} \alpha_n(-\pi, \phi) = \frac{1}{2\pi} \phi + \frac{1}{2}$.

5.3. Yang-Lee zeros (a -plane zeros of $G_N(a, t)$)

The Yang-Lee zeros (see section 4.3) of the partial generating function $G_N(a, t)$ (equation (14)) are closely related to Fisher (partition function) zeros. These zeros were estimated using Maple [36], and are plotted for $N \in \{100, 200, 300, 400, 500\}$ in figure 28.

The distribution of Yang-Lee zeros, and their other properties, are very similar to those of Fisher zeros; see section 4.2. The data in figure 28 are for $t = \frac{1}{\mu_3}$, and it is found that the locations of the zeros, and their distribution, are not very sensitive to changes in t (the data in figure 28 are very similar to the data shown in figure 24). In addition, the position and trajectory of the leading zero is very similar to the data in figure 26, while the cumulative angular distribution of zeros has the same profile as seen in figure 27.

5.4. The density profile and distribution of Fisher and Yang-Lee zeros

The angular and radial distribution of partition function zeros in figure 24, or Yang-Lee zeros in figure 28, are similar. The angular distribution of partition function zeros was examined in figure 27, where the cumulative angular distribution function is shown. Yang-Lee zeros of $G_N(a, t)$ have a cumulative distribution which is similar to figure 27, and it is not shown here.

The angular distribution of zeros may also be examined by counting zeros in wedges around the origin. If the plane is partitioned by M wedges at the origin in the a -plane with vertex angles of size $\frac{2\pi}{M}$, then the angular distribution can be estimated by counting zeros in each wedge. Binning the partition function zeros for each wedge, and plotting the results against bin number gives figure 29 (where $M = 50$ and for $n \in \{100, 200, \dots, 500\}$). The darker colours correspond to larger values

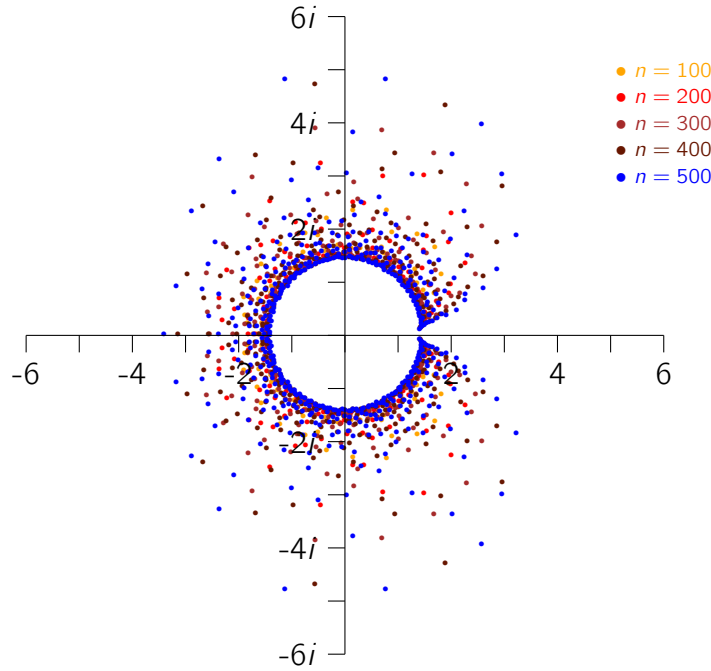


Figure 28: Zeros of $G_N(a, t)$ (Yang-Lee zeros) for adsorbing walks in the cubic lattice in the a -plane for $t = \frac{1}{\mu_3}$. This distribution of the zeros is similar to that seen for Fisher zeros (see figure 24). Examination of the data show that this pattern of zeros is not very sensitive to the value of t in the generating function. With increasing N the leading zero and its conjugate approaches the positive real axis at the adsorption critical point a_c^+ , creating an edge singularity in the limit as $N \rightarrow \infty$.

of n , and the figure is obtained by plotting $\frac{50}{2\pi n} \alpha_n(\frac{(2m-1)\pi}{100}, \frac{(2m+1)\pi}{100})$ against $\frac{2m\pi}{50}$ for $m = -25, -24, \dots, 25$, with the points interpolated by line segments. The graph is very uneven for small n , but this unevenness subsides as n increases. Also notable is the low density in a (narrow) wedge containing the positive real axis.

Plotting Yang-Lee zeros instead of partition function zeros gives very similar looking results.

In the radial direction the partition function zeros appear to accumulate on a circle $|a| = a_c^+$ in the a -plane with increasing n . The fraction of zeros inside a disk $|a| < r$, or outside disks $|a| < r$, is a function of n , but this may be approaching limiting values as n increases to infinity. This possibility is examined in figure 30. The data points marked by $|a| \leq 1.45$ in this figure correspond to the fraction of zeros inside the disk $|a| \leq 1.45$ (this is the same as the fraction of zeros inside the annulus $a_c^+ \leq |a| \leq 1.45$). The fraction is small for $n < 150$, but increases steadily and seems to approach a constant value of about 0.30 for $n > 300$.

A similar situation is seen for zeros farther away from the origin. For example, the fraction of zeros farther away than a distance of 1.45 from the origin (that is, the fraction of zeros *outside* a disk $|a| \leq 1.45$ at the origin), is shown by the data points accumulating along the top curve of the graph in figure 30. For small values of n the fraction is nearly equal to 1, but this decreases and levels off at a density of about 0.70 for $n > 300$.

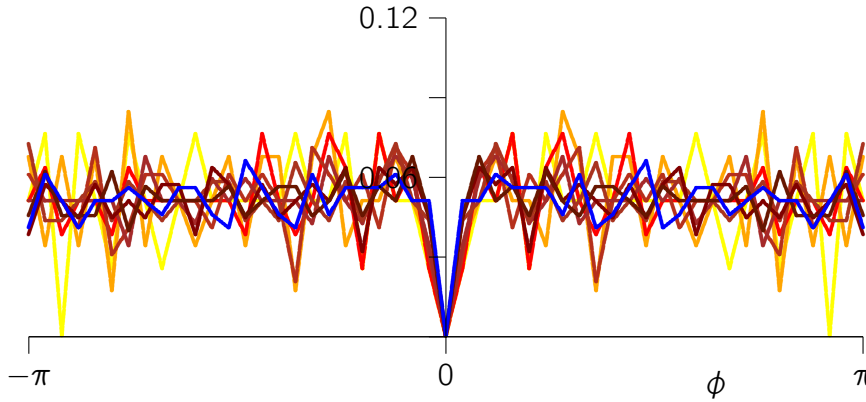


Figure 29: The angular distribution of partition function zeros in the cubic lattice estimated by plotting $\frac{50}{2\pi n} \alpha_n(\frac{(2m-1)\pi}{100}, \frac{(2m+1)\pi}{100})$ against $\frac{2m\pi}{50}$ for $m = -25, -24, -23, -22, \dots, 24, 25$, and for $n \in \{100, 200, \dots, 500\}$. The darker colours correspond to larger values of n , and the data points are interpolated by line segments. The data become less noisy with increasing n , and there is a notable decrease (to zero) of the density of zeros close to the positive real axis (where $\phi = 0$).

The density outside disks $|a| \leq r$ decreases with increasing r , as seen for $r \in \{1.45, 1.55, 1.65, 1.75\}$ in figure 30. In each case the fraction of zeros levels off (within noise) to a constant, independent of n . The results for Yang-Lee zeros (zeros of $G_N(a, t)$ with $t = \frac{1}{\mu_2}$) are similar to the results for partition function zeros shown in figure 30.

Similar to the observation for adsorbing square lattice walks, the results in figure 30 suggest that only a fraction of Fisher and Yang-Lee zeros accumulate on the critical circle $|a| = a_c^+$. That is, it appears that a constant fraction of zeros accumulate on the critical circle, while the inside of the critical circle is empty. The radial density (integrated in the angular direction) approaches a constant value with increasing n . This suggests, in the limit as $n \rightarrow \infty$, that there are zeros at arbitrary distances from the origin. However, since the distribution of zeros is integrable, the *number density* of zeros should drop off faster than the inverse squared distance from the origin.

6. Conclusions

In this paper the properties of partition and generating functions zeros of models of adsorbing walks in the square and cubic lattices were examined numerically. In addition, it was shown that theorems on the distribution of polynomial zeros can be used to prove theorems on the distribution of partition and generating function zeros in these models. This includes theorem 2.2, which shows that generating function zeros in the t -plane converge on a circle – these are the Lee-Yang zeros, and by theorem 2.4 they converge to a uniform distribution in the limit as the length of the walk approaches infinity. These results are corollaries of the theorem of Hughes and Nikechbali (theorem 2.1), and the theorems of Erdős and Turán (theorem 2.3) and Erdélyi (theorem 2.10).

Numerical results on the Lee-Yang zeros in the t -plane were given in sections 4.1 and 5.1. The results show that the zeros are distributed evenly on a circle of radius λ_a^{-1} , even for small values of N as seen in figures 2, 7, 8 and 9 for square lattice adsorbing

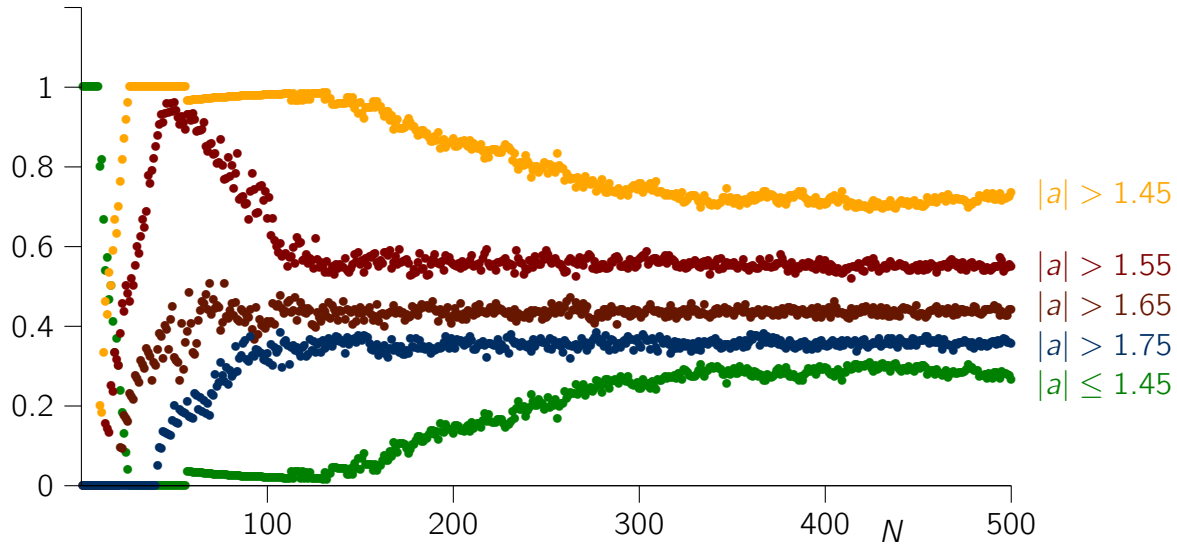


Figure 30: The fraction of partition function zeros (zeros of $A_n^+(a)$ in the a -plane) of adsorbing walks in the cubic lattice. The data displayed show the fraction of zeros at distances closer than 1.45 (green points along the lowest curve), and then farther away than 1.45, 1.55, 1.65 and 1.75 from the origin in the a -plane. Determining the same data for Yang-Lee zeros (zeros of $G_N(a, t)$ with $t = \frac{1}{\mu_3}$) gives similar results, with data points which largely coincide with the data plotted here. The data appear to flatten out to constant values with increasing n . This implies that the number density of zeros decreases inversely with distance from the origin if $|a|$ is large and in the limit that $n \rightarrow \infty$.

walks, and figures 19, 20, 21 and 22 for cubic lattice adsorbing walks. Moreover, the zeros of the generating function $G_N(a, t)$ were seen to be close to N vertices of a regular $(N+1)$ -gon. As N increases this gives an increasingly uniform distribution of the zeros on the circle.

The distribution of partition function (or Fisher) zeros was also examined. These zeros were shown to be distributed with positive density in an annulus in the complex a -plane in theorem 2.8. The angular distribution of Fisher zeros was also considered by examining the function $\alpha_n(\theta, \phi)$. This, in particular, gives, in the limit as $n \rightarrow \infty$, an angular distribution $q(\theta)$, as defined in equation (54). Bounds on $q(\theta)$ are given in theorem 2.11.

Numerical results on the distribution of Fisher zeros are consistent with the theorems in section 2.3. The distribution of Fisher zeros is typically similar to the data shown in figures 10, 11 and 12 for square lattice adsorbing walks, and figures 23 and 24 for cubic lattice adsorbing walks. It was shown that thermodynamic quantities (the free energy, energy and specific heat) can be computed from the Fisher zeros (see figures 13 and 25) and that these are consistent with results obtained by other means; see for example reference [24]. The trajectory of the leading Fisher zero a_1 in figures 14 and 26 follows an approximately parabolic path with increasing length of the walk, and approaches the real axis at an angle which was estimated to be about 55° in the square lattice. Estimating this angle in the cubic lattice proved more difficult. If the estimate $a_c^\pm = 1.306$ for the critical value of a is used, then the angle has a value of approximately 55° . If this is not used, then the angle appears to be larger, for example, approximately 64° in figure 26.

The cumulative angular distribution function of Fisher zeros is illustrated in figure 15 for square lattice adsorbing walks, and figure 27 for cubic lattice adsorbing walks. There is very little difference in these figures, and with increasing n both cases appear to approach the linear function $\frac{1}{2\pi}\phi + \frac{1}{2}$. That is, the angular distribution is a constant function away from the angle $\phi = 0$ in the limit as $n \rightarrow \infty$. This is consistent with the graphs in figures 17 and 29, which becomes less noisy with increasing n .

The radial distributions of Fisher zeros were also plotted in figures 18 and 30. The fraction of zeros outside disks of given radius r approaches a constant as n increases, showing that the number density of Fisher zeros decreases with increasing distance from the origin in the a -plane.

Results on the distribution of Yang-Lee zeros in the a -plane were similarly presented. These zeros are distributed similarly to Fisher zeros, and the results in theorems 2.12 on the radial distribution is similar to the radial distribution of Fisher zeros seen in theorem (2.8). The angular distribution of Yang-Lee zeros was also seen to be similar to that of Fisher zeros, and the results on the distribution function are given in theorem 2.14. Numerical investigation on the Yang-Lee zeros produced results similar to that seen for Fisher zeros.

Acknowledgements: EJJvR acknowledges financial support from NSERC (Canada) in the form of a Discovery Grant.

References

- [1] MT Batchelor and CM Yung. Exact results for the adsorption of a flexible self-avoiding polymer chain in two dimensions. *Phys Rev Lett*, 74:2026–2029, 1995.
- [2] NR Beaton, AJ Guttmann, and I Jensen. Two-dimensional self-avoiding walks and polymer adsorption: Critical fugacity estimates. *J Phys A: Math Theo*, 45:055208, 2012.
- [3] D Bennett-Wood and AL Owczarek. Exact enumeration results for self-avoiding walks on the honeycomb lattice attached to a surface. *J Phys A: Math Gen*, 29:4755–4768, 1996.
- [4] HJ Brascamp and H Kunz. Zeros of the partition function for the ising model in the complex temperature plane. *Journal of Mathematical Physics*, 15(1):65–66, 1974.
- [5] TW Burkhardt, E Eisenriegler, and I Guim. Conformal theory of energy correlations in the semi-infinite two-dimensional $O(n)$ model. *Nucl Phys B*, 316:559–572, 1989.
- [6] JL Cardy. Conformal Invariance. In C Domb and JL Lebowitz, editors, *Phase Transitions and Critical Phenomena*, volume 11, pages 55–126, 1983.
- [7] JL Cardy. Conformal invariance and the Yang-Lee edge singularity in two dimensions. *Phys Rev Lett*, 54(13):1354–1356, 1985.
- [8] N Clisby. Calculation of the connective constant for self-avoiding walks via the pivot algorithm. *J Phys A: Math Theo*, 46:245001, 2013.
- [9] N Clisby, AR Conway, and AJ Guttmann. Three-dimensional terminally attached self-avoiding walks and bridges. *J Phys A: Math Theo*, 49(1):015004, 2015.
- [10] N Clisby and I Jensen. A new transfer-matrix algorithm for exact enumerations: Self-avoiding polygons on the square lattice. *J Phys A: Math Theo*, 45:115202, 2012.
- [11] T Erdélyi. An improvement of the Erdős-Turán theorem on the distribution of zeros of polynomials. *CR Acad Sci Paris, Ser I*, 346:267–270, 2008.
- [12] P Erdős and P Turán. On the distribution of roots of polynomials. *Ann Math*, 51(1):105–119, 1950.
- [13] ME Fisher. Correlation functions and the critical region of simple fluids. *J Math Phys*, 5(7):944–962, 1964.

- [14] ME Fisher. Lectures in Theoretical Physics. Vol VII C (U Colorado Press 1965), 1965.
- [15] ME Fisher. Yang-Lee edge singularity and ϕ^3 field theory. *Phys Rev Lett*, 40(25):1610–1613, 1978.
- [16] P Grassberger. Pruned-enriched Rosenbluth method: Simulations of θ polymers of chain length up to 1000000. *Phys Rev E*, 56:3682–3693, 1997.
- [17] JM Hammersley. Percolation processes. II The connective constant. *Proc Camb Phil Soc*, 53:642–645, 1957.
- [18] JM Hammersley, GM Torrie, and SG Whittington. Self-avoiding walks interacting with a surface. *J Phys A: Math Gen*, 15:539–571, 1982.
- [19] R Hegger and P Grassberger. Chain polymers near an adsorbing surface. *J Phys A: Math Gen*, 27:4069–4081, 1994.
- [20] CP Hughes and A Nikeghbali. The zeros of random polynomials cluster uniformly near the unit circle. *Compositio Mathematica*, 144(03):734–746, 2008.
- [21] EJ Janse van Rensburg. Collapsing and adsorbing polygons. *J Phys A: Math Gen*, 31(41):8295–8306, 1998.
- [22] EJ Janse van Rensburg. Approximate enumeration of self-avoiding walks. *Algorithmic Probability and Combinatorics*, 520:127–151, 2010.
- [23] EJ Janse van Rensburg. *The Statistical Mechanics of Interacting Models of Self-Avoiding Walks, Polygons, Animals and Vesicles*. Oxford University Press, 2015.
- [24] EJ Janse van Rensburg. Microcanonical simulations of adsorbing self-avoiding walks. *J Stat Mech: Theo Expr*, 2016(3):033202, 2016.
- [25] EJ Janse van Rensburg and A Rechnitzer. Multiple Markov chain Monte Carlo study of adsorbing self-avoiding walks in two and in three dimensions. *J Phys A: Math Gen*, 37:6875–6898, 2004.
- [26] EJ Janse van Rensburg and A Rechnitzer. Generalized atmospheric sampling of self-avoiding walks. *J Phys A: Math Theo*, 42:335001, 2009.
- [27] I Jensen. Enumeration of self-avoiding walks on the square lattice. *J Phys A: Math Gen*, 37:5503–5524, 2004.
- [28] S-Y Kim and RJ Creswick. Yang-Lee zeros of the q -state Potts model in the complex magnetic field plane. *Phys Rev Lett*, 81(10):2000–2003, 1998.
- [29] S-Y Kim and RJ Creswick. Density of states, Potts zeros, and Fisher zeros of the q -state Potts model for continuous q . *Phys Rev E*, 63(6):066107, 2001.
- [30] S-Y Kim and Creswick RJ. Fisher zeros of the q -state Potts model in the complex temperature plane for non-zero external magnetic field. *Phys Rev E*, 58:7006–7012, 1998.
- [31] DA Kurtze and ME Fisher. Yang-Lee edge singularities at high temperatures. *Phys Rev B*, 20(7):2785–2796, 1979.
- [32] J Lee. Exact partition function zeros of two-dimensional lattice polymers. *J Korean Phys Soc*, 44(1):617–620, 2004.
- [33] T-D Lee and C-N Yang. Statistical theory of equations of state and phase transitions. II Lattice gas and Ising model. *Phys Rev*, 87(3):410–419, 1952.
- [34] S Livne and H Meirovitch. Computer simulation of long polymers adsorbed on a surface. I Corrections to scaling in an ideal chain. *J Chem Phys*, 88:4498–4506, 1988.
- [35] L Ma, KM Middlemiss, GM Torrie, and SG Whittington. Location of the adsorption transition for polymers with excluded volume. Monte Carlo and enumeration results. *J Chem Soc, Farad Trans 2: Mol Chem Phys*, 74:721–726, 1978.
- [36] Maplesoft. *Maple 17*. A division of Waterloo Maple Inc. (Waterloo Ontario).
- [37] H Meirovitch and S Livne. Computer simulation of long polymers adsorbed on a surface. II Critical behavior of a single self-avoiding walk. *J Chem Phys*, 88:4507–4515, 1988.
- [38] G Parisi and N Sourlas. Critical behavior of branched polymers and the Lee-Yang edge singularity. *Phys Rev Lett*, 46(14):871–874, 1981.
- [39] T Prellberg and J Krawczyk. Flat histogram version of the pruned and enriched Rosenbluth method. *Phys Rev Lett*, 92:120602, 2004.
- [40] JCS Rocha, S Schnabel, DP Landau, and M Bachmann. Leading Fisher partition function zeros as indicators of structural transitions in macromolecules. *Physics Procedia*, 57:94–98, 2014.
- [41] D Ruelle. *Statistical Mechanics*. Addison-Wesley, 4 edition, 1983.

- [42] MP Taylor, PP Aung, and W Paul. Partition function zeros and phase transitions for a square-well polymer chain. *Phys Rev E*, 88(1):012604, 2013.
- [43] MP Taylor and J Luettmmer-Strathmann. Partition function zeros and finite size scaling for polymer adsorption. *J Chem Phys*, 141(20):204906, 2014.
- [44] C-N Yang and T-D Lee. Statistical theory of equations of state and phase transitions. I Theory of condensation. *Phys Rev*, 87(3):404–409, 1952.